Bone 181 (2024) 117044

Contents lists available at ScienceDirect

Bone

journal homepage: www.elsevier.com/locate/bone

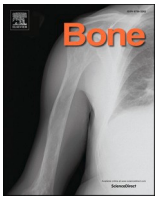

Full Length Article

Complex intrinsic abnormalities in osteoblast lineage cells of X-linked hypophosphatemia: Analysis of human iPS cell models generated by CRISPR/Cas9-mediated gene ablation

Tatsuro Nakanishi [a,b], Miwa Yamazaki [a], Kanako Tachikawa [a], Ayu Ueta [a,c], Masanobu Kawai [a], Keiichi Ozono [d], Toshimi Michigami [a,*]

[a] Department of Bone and Mineral Research, Research Institute, Osaka Women's and Children's Hospital, Osaka Prefectural Hospital Organization, Izumi, Osaka 594-1101, Japan
[b] Department of Pediatrics, Osaka University Graduate School of Medicine, Suita, Osaka 565-0871, Japan
[c] 1st Department of Oral and Maxillofacial Surgery, Osaka University Graduate School of Dentistry, Suita, Osaka 565-0871, Japan
[d] Professor Emeritus, Osaka University, Japan

ARTICLE INFO

Keywords:
Phosphate regulating endopeptidase homolog X-linked
Osteoblast
Osteocyte
Induced pluripotent stem cell
Phosphate

ABSTRACT

X-linked hypophosphatemia (XLH) is caused by inactivating variants of the *phosphate regulating endopeptidase homolog X-linked* (*PHEX*) gene. Although the overproduction of fibroblast growth factor 23 (FGF23) is responsible for hypophosphatemia and impaired vitamin D metabolism, the pathogenesis of XLH remains unclear. We herein generated *PHEX*-knockout (KO) human induced pluripotent stem (iPS) cells by applying CRISPR/Cas9-mediated gene ablation to an iPS clone derived from a healthy male, and analyzed *PHEX*-KO iPS cells with deletions extending from exons 1 to 3 and frameshifts by inducing them to differentiate into the osteoblast lineage. We confirmed the increased production of FGF23 in osteoblast lineage cells differentiated from *PHEX*-KO iPS cells. *In vitro* mineralization was enhanced in osteoblast lineage cells from *PHEX*-KO iPS cells than in those from isogenic control iPS cells, which reminded us of high bone mineral density and enthesopathy in patients with XLH. The extracellular level of pyrophosphate (PPi), an inhibitor of mineralization, was elevated, and this increase appeared to be partly due to the reduced activity of tissue non-specific alkaline phosphatase (TNSALP). Osteoblast lineage cells derived from *PHEX*-KO iPS cells also showed the increased expression of multiple molecules such as dentine matrix protein 1, osteopontin, RUNX2, FGF receptor 1 and early growth response 1. This gene dysregulation was similar to that in the osteoblasts/osteocytes of *Phex*-deficient *Hyp* mice, suggesting that common pathogenic mechanisms are shared between human XLH and *Hyp* mice. Moreover, we found that the phosphorylation of CREB was markedly enhanced in osteoblast lineage cells derived from *PHEX*-KO iPS cells, which appeared to be associated with the up-regulation of the *parathyroid hormone related protein* gene. *PHEX* deficiency also affected the response of the *ALPL* gene encoding TNSALP to extracellular Pi. Collectively, these results indicate that complex intrinsic abnormalities in osteoblasts/osteocytes underlie the pathogenesis of human XLH.

1. Introduction

X-linked hypophosphatemia (XLH, OMIM #307800) is the most frequent form of hereditary hypophosphatemic rickets/osteomalacia with a frequency of approximately 1 case in 20,000 live births, and is inherited in an X-linked dominant manner [1,2]. Patients with XLH have an increased level of circulating fibroblast growth factor 23 (FGF23), which leads to renal phosphate wasting, hypophosphatemia, and low to inappropriately normal levels of serum 1,25-dihydroxyvitamin D (1,25$(OH)_2$D) [2,3]. FGF23 is mainly produced by mature osteoblasts as well as osteocytes which are the terminally differentiated cells of the osteoblast lineage, and exerts its effects on distant target tissues in an endocrine manner. In the kidneys which are its main target, FGF23 increases the excretion of inorganic phosphate (Pi) by suppressing the expression of type IIa and IIc sodium/phosphate (Na^+/Pi) co-transporters, and decreases the production of 1,25$(OH)_2$D by down-regulating 25-

* Corresponding author.
E-mail address: michigami@wch.opho.jp (T. Michigami).

https://doi.org/10.1016/j.bone.2024.117044
Received 16 November 2023; Received in revised form 4 January 2024; Accepted 5 February 2024
Available online 6 February 2024

hydroxyvitamin D 1α-hydroxylase and up-regulating 25-hydroxyvitamin D-24-hydroxylase [4]. In addition to hypophosphatemic rickets/osteomalacia, patients with XLH may develop complications such as dental abscesses and enthesopathy.

XLH is caused by inactivating variants in the *phosphate regulating endopeptidase homolog X-linked* (*PHEX*) gene located at Xp22.1. To date, >1000 *PHEX* variants have been identified and are listed in the *PHEX* Locus Specific Database (https://www.rarediseasegenes.com/) [5]. The *PHEX* gene consists of 22 exons and is suggested to encode a type 2 membrane protein that exhibits a single transmembrane structure [6]. It is predominantly expressed in osteoblasts and osteocytes as well as in odontoblasts and cementoblasts [7]. In mouse bone, *Phex* and *Fgf23* were both found to be expressed in osteoblast lineage cells with higher expression in osteocytes [8]. The putative structure of the *PHEX* product suggests a function as a zinc-dependent endopeptidase [9]; however, its physiological roles remain largely unknown. Although serum FGF23 levels are elevated in XLH patients, FGF23 does not serve as a substrate for PHEX [10]. Therefore, the regulation of FGF23 by PHEX may be indirect and involve other molecule(s).

To date, the pathogenesis of XLH has mainly been investigated using mouse models. Hypophosphatemic *Hyp* mice harbor a large 3′-deletion in the *Phex* gene and are widely used as a model of human XLH, showing elevated FGF23 levels, hypophosphatemia and impaired skeletal mineralization [11,12]. An analysis of conditional knockout (KO) mice in which the *Phex* gene was ablated using the *osteocalcin*-Cre driver have suggested that *PHEX* deficiency in osteoblast lineage cells is sufficient to induce the *Hyp* phenotype [13]. Previous studies using *Hyp* mice revealed that *Phex*-deficient osteoblast lineage cells may have complex defects in addition to the increased production of FGF23. For example, the extracellular matrix protein osteopontin (OPN) was shown to accumulate in the bones of *Hyp* mice, and the genetic elimination of OPN in *Hyp* mice partially restored defective bone mineralization without addressing hypophosphatemia [14,15]. In our previous studies using osteoblasts and osteocytes freshly isolated from *Hyp* mice and wild-type (WT) littermates, we found that the expression of *dentin matrix protein 1* (*Dmp1*) and *family with sequence similarity, member c*, the causative genes for autosomal recessive hypophosphatemic type 1 (ARHR1) and Raine syndrome (RNS), respectively, were markedly up-regulated in *Hyp* cells [8]. In addition, FGFR signaling was enhanced in osteocytes of *Hyp* mice in association with the up-regulation of canonical FGF ligands and FGF receptors [8,16], and the conditional KO of *Fgfr1* in mature osteoblasts and osteocytes using the *Dmp1*-Cre driver was shown to partially restore elevated FGF23 and hypophosphatemia in *Hyp* mice [17].

These findings imply that multiple abnormalities in osteoblast lineage cells may contribute to the pathogenesis of *Hyp* mice; however, it remains unclear whether a similar mechanism applies to human XLH, partly due to the difficulties associated with obtaining a sufficient number of osteoblast lineage cells for analyses from human bone specimens. Human induced pluripotent stem cells (iPSCs) provide new *in-vitro* models for skeletal diseases [18,19]. Therefore, to investigate the precise mechanisms underlying the pathogenesis of human XLH, we herein generated human iPSCs deficient for *PHEX* by applying CRISPR/Cas9-mediated gene ablation to healthy male-derived iPSCs. An analysis of the osteoblast lineage cells differentiated from *PHEX*-KO iPSCs and those from isogenic control iPSCs, which are genetically identical except for the *PHEX* gene, revealed that multiple intrinsic abnormalities in osteoblast lineage cells contribute to the pathogenesis of human XLH.

2. Materials and methods

2.1. Cell culture

The human iPS cell line 610B1 derived from the umbilical cord blood cells of a human male was provided by the RIKEN BRC (Tsukuba, Japan) through the National BioResource Project of the MEXT/AMED, Japan. iPSCs were maintained under feeder-free conditions on recombinant laminin fragment iMatrix-511 Silk (Matrixome, Osaka, Japan) using StemFit® AK02N medium (Ajinomoto, Tokyo, Japan) at 37 °C in a 5 % CO_2 atmosphere. To detach adherent iPSCs, they were treated with TrypLE™ Express (Thermo Fisher Scientific, Waltham, MA, USA). The ROCK inhibitor Y-27632 (10 mM, Selleck Chemicals, Houston, TX, USA) was added to the medium until the next day of cell plating in order to prevent dissociation-induced cell apoptosis.

2.2. Generation of PHEX-KO human iPSCs by CRISPR/Cas9-mediated gene ablation

To generate human iPSCs deficient for the *PHEX* gene, we applied CRISPR/Cas9-mediated gene ablation to the 610B1 iPS cell line derived from a healthy human male, which carried a single allele of *PHEX*. Two synthetic single guide RNAs (sgRNAs) targeted to exons 1 and 3 of *PHEX*, respectively, were transfected into cells together with the recombinant Cas9 protein (TrueCut™ Cas9 Protein v2, Thermo Fisher Scientific) using Lipofectamine CRISPRMAX™ Cas9 Transfection Reagent (Thermo Fisher Scientific). The target sequence for *PHEX* exon 1 was 5'- GAGGATCGTGCCCAGAACTA-3', and that for exon 3 was 5'-TTCTTCCGGTTCGCTTGTGA-3'. Two days after transfection, cells were detached and plated on 96-well culture plates for single cell cloning by limiting dilutions. *PHEX*-KO clones were selected by a genomic polymerase chain reaction (PCR), which amplified the fragments containing the target regions and sequencing. Gel-purified PCR products were sequenced after being cloned into the pT7-Blue vector (Novagen, Madison, WI, USA).

To verify the successful ablation of functional transcripts of *PHEX*, we performed reverse transcription-PCR (RT-PCR). Total RNA was extracted using TRIzol Reagent (Thermo Fisher Scientific), treated with DNase (Qiagen, Tokyo, Japan), and then reverse-transcribed using random hexamers (Promega, Madison, WI, USA) and SuperScript II reverse transcriptase (Thermo Fisher Scientific). The primer sequences for genomic PCR and RT-PCR are shown in Supplemental Table S1.

2.3. Assay for cell viability and cytotoxicity

iPSCs were seeded at 0.5×10^3 or 1×10^3 cells/well on 96-well plates coated with iMatrix-511 silk (1.0 μg/cm^2) and cultured in StemFit® AK02N medium. The numbers of live cells and dead cells in each well were assessed using the MultiTox-Fluor Multiplex Cytotoxicity Assay (Promega).

2.4. Osteogenic induction of human iPSCs

The differentiation of human iPSCs to the osteoblast lineage was induced according to the protocol reported by Kawai et al. [18] with modifications. iPSCs maintained under feeder-free conditions were detached and plated at 4×10^5 cells/well on 12-well culture plates coated with iMatrix-511 silk (1.0 μg/cm^2). Cells were cultured in a mixture of 20 % StemFit® AK02N feeder-free medium and 80 % osteogenic induction medium composed of KnockOut-DMEM (Thermo Fisher Scientific), supplemented with 20 % fetal bovine serum (FBS: Sigma-Aldrich, St. Louis, MO), 10 mM β-glycerophosphate (Sigma-Aldrich), 1 nM dexamethasone (Sigma-Aldrich), 0.1 mM 2-mercaptoethanol (Thermo Fisher Scientific), 50 μg/mL L-ascorbic acid 2-phosphate sesquimagnesium salt hydrate (Nacalai Tesque Inc., Kyoto, Japan), 1 % non-essential amino acids (Thermo Fisher Scientific), 2 mM L-glutamine (Thermo Fisher Scientific) and 1 μM all-trans retinoic acid (Fujifilm Wako, Osaka, Japan), in the presence of 10 μM Y-27632. Two days later, the medium was replaced with 100 % osteogenic induction medium without Y-27632. Cells were cultured up to 49 days with medium being refreshed every 2 or 3 days.

2.5. Measurement of intact FGF23 levels in conditioned media

iPSCs were induced to differentiate to osteoblast lineage cells for 49 days as described above. Cells were then incubated in fresh media for an additional 72 h to harvest conditioned media for the measurement of intact FGF23 levels using an ELISA kit (Kainos Laboratories, Tokyo, Japan). The amount of FGF23 in conditioned media was standardized to the protein content of cell lysates.

2.6. Assays for in vitro mineralization

To assess the *in vitro* mineralization ability of osteoblast lineage cells differentiated from iPSCs, Alizarin red staining and the OsteoImage™ Mineralization Assay (Lonza, Basel, Switzerland) were performed. Regarding Alizarin red staining, cells in culture were washed twice with phosphate-buffered saline (PBS) and then fixed in 95 % methanol at room temperature for 20 min. Fixed cells were then repeatedly washed with water and stained with 40 mM Alizarin red S (Sigma-Aldrich, pH 5.4) at room temperature for 20 min. Stained cells were washed thoroughly and air dried. Alizarin red-positive areas were measured using ImageJ software.

The OsteoImage™ Mineralization Assay (Lonza) specifically quantitates hydroxyapatite. According to the manufacturer's instructions, hydroxyapatite was stained with OsteoImage™ fluorescent dye and quantified on a fluorescence plate reader using 492 nm excitation and 520 nm emission wavelengths.

2.7. Isolation of osteoblast/osteocyte lineage cells from mouse bones

In some experiments, we analyzed osteoblasts and osteocytes that were freshly isolated from mouse bones. Animal experiments were performed in accordance with the "Guidelines for Proper Conduct of Animal Experiments" formulated by the Scientific Council of Japan, after the approval of protocols by the Institutional Animal Care and Use Committee of Osaka Women's and Children's Hospital (Permit number: BMR-2020-1). *Phex*-deficient *Hyp* mice were initially obtained from the Jackson Laboratory (Bar Harbor, ME, USA) and were bred to produce male hemizygotes ($Phex^{Hyp}/Y$) and their WT littermates. All mice were fed standard mouse chow (CE-2; CLEA Japan) and tap water *ad libitum* and were maintained under a 12-hour light/dark cycle.

Primary osteoblasts and osteocytes were isolated from the femurs and tibiae of 10-week-old male *Hyp* mice and WT littermates as we previously reported [8,20,21]. Briefly, minced bones were sequentially digested with 1.25 mg/mL collagenase (Fujifilm Wako) in Ca^{2+}-free, Mg^{2+}-free Hanks' Balanced Salt Solution (HBSS) at 37 °C for 15 min twice (first and second rounds) and then for 20 min three times (third to fifth rounds). After each step of digestion, cells released from bone were collected through a 100-μm nylon cell strainer as Fractions 1 to 5, respectively. Bone pieces were then decalcified with 4 mM ethylene glycol tetraacetic acid (EGTA) in HBSS for 15 min and then digested with 1.25 mg/mL collagenase for 20 min to harvest cells as Fractions 6 and 7, respectively. This procedure was repeated to collect cells as Fractions 8 and 9. Based on the expression profiles of marker genes, Fractions 3–5 were considered to be rich in osteoblasts, while Fractions 6–9 were rich in osteocytes [8,20]. The volumes of collagenase solution and EGTA solution were adjusted according to the body weight of mice.

2.8. Real-time RT-PCR analysis

To quantify mRNA expression, real-time RT-PCR was performed using TaqMan® Gene Expression Assays and the StepOne Plus Real-Time PCR System (Applied Biosystems, Foster city, CA, USA). In the analysis of *PHEX* expression, we also performed SYBR Green I-based real-time PCR using the primers shown in Supplemental Table S1. To generate a standard curve, serial 10-fold dilutions of the pT7-Blue vector (Novagen) containing the amplicon of interest were included in the assay. The copy number of the target cDNA was estimated by referring to the standard curve and was standardized to that of *Gapdh* cDNA in each sample.

2.9. Western blotting

Whole cell lysates were prepared in RIPA buffer containing 1 % Triton, 1 % Na deoxycholate, 0.1 % SDS, 150 mM NaCl, 10 mM Tris-Cl (pH 7.4), 5 mM EDTA, orthovanadate, NaF and the protease inhibitor cocktail Complete™ (Roche Diagnostics, Mannheim, Germany). Equal amounts of protein were separated on SDS-PAGE and were transferred to PVDF membranes (BioRad Laboratories, Hercules, CA). After blocking with Blocking One P reagent (Nacalai Tesque Inc.) or Block Ace reagent (Dainippon Pharmaceuticals, Osaka, Japan), the membranes were incubated at 4 °C overnight with the following primary antibodies: anti-DMP1 rabbit polyclonal antibody (TaKaRa, Shiga, Japan), anti-OPN rabbit polyclonal antibody (ProteinTech, Rosemont, IL, USA), anti-PiT1 (SLC20A1) rabbit polyclonal antibody (H-130; Santa Cruz Biotechnology, Santa Cruz, CA), anti-SLC20A2 (PiT-2) rabbit polyclonal antibody (ProteinTech), anti-GAPDH goat polyclonal antibody (V-18; Santa Cruz Biotechnology), anti-phosphorylated ERK1/2 antibody, anti-ERK1/2 antibody, anti-phosphorylated CREB (Ser133) antibody, anti-CREB antibody, anti-phosphorylated FRS2α antibody (Cell Signaling Technology, Beverly, MA, USA), and anti-FRS2α antibody (Santa Cruz Biotechnology). Membranes were then incubated with the corresponding horseradish peroxidase (HRP)-conjugated secondary antibodies, followed by signal detection using the enhanced chemiluminescence system (GE Healthcare, Buckinghamshire, UK). Densitometry was performed using ImageJ software to quantify signal intensities.

2.10. Measurement of extracellular pyrophosphate (PPi), ATP, and Pi levels

iPSCs were induced to differentiate into osteoblast lineage cells for 49 days. The medium was then refreshed, followed by the collection of 72-hour conditioned media and cell lysates. PPi in conditioned media, which was regarded as extracellular PPi, was assayed using a PPi Assay kit (BioVision, Milpitas, CA, USA) and standardized to the protein content of cell lysates. We also measured adenosine triphosphate (ATP) levels in conditioned media using a CellTiter-Glo® 2.0 Assay kit (Promega). Pi concentrations in conditioned media were assayed using a Phospho-C test kit (Fujifilm Wako).

2.11. Measurement of tissue non-specific alkaline phosphatase (TNSALP) enzymatic activity

Cell lysates were harvested in RIPA buffer from *PHEX*-KO and isogenic control 610B1 iPSCs on Day 49 of osteogenic induction. TNSALP activity in lysates was assayed using *p*-nitrophenylphosphate as a substrate in glycine alkaline buffer containing $MgCl_2$. The reaction was performed at 37 °C for 30 min, and TNSALP activity was assessed by referring to a *p*-nitrophenol (*p*-NP) standard and normalized to the protein content in each sample.

ALP activity was also visualized by ALP cell staining. Cells in culture were washed once with PBS and then fixed in 3.7 % formaldehyde solution at 4 °C for 10 min. Fixed cells were then repeatedly washed with PBS and stained with premixed ALP substrate solution (Fujifilm Wako) at 37 °C for 30 min. Stained cells were washed with water thoroughly and air dried. Positively stained areas were measured using ImageJ software.

2.12. Statistical analysis

The Mann-Whitney *U* test was performed to compare data between 2 groups. To compare data among 3 or more groups, we used a one-way analysis of variance (ANOVA) and Tukey-Kramer's and Dunnett's *post*

hoc tests.

3. Results

3.1. Induction of PHEX expression by the differentiation of control iPSCs into the osteoblast lineage

We initially confirmed the induction of *PHEX* expression by the osteoblastic differentiation of control iPSCs. The 610B1 iPSC clone derived from a healthy male was subjected to osteogenic differentiation, as described in Methods Section 2.4., up to Day 49 (Fig. 1A). RNA was extracted on Days 14, 28, and 49 to examine time changes in the expression of *RUNX2* and *PHEX*. The expression of *RUNX2*, the gene encoding the master transcription factor for osteoblast differentiation, peaked on Day 28 and then declined. On the other hand, the expression of *PHEX* was detected on Day 14 and increased up to Day 49 (Fig. 1B). Alizarin red staining revealed a gradual increase in mineralized nodules (Fig. 1C). We also confirmed the accumulation of hydroxyapatite using OsteoImage™ fluorescent dye, which specifically binds to hydroxyapatite (Fig. 1D). These results verified that 610B1 iPSCs were successfully induced to differentiate into the osteoblast lineage and acquired the expression of *PHEX*.

3.2. Generation of PHEX-KO human iPSCs by CRISPR/Cas9-mediated gene ablation

We applied CRISPR/Cas9-mediated gene ablation to 610B1 iPSCs in order to generate iPSCs deficient for the *PHEX* gene. Since the 610B1 iPS clone is derived from a healthy male, it carries only one allele of the *PHEX* gene locus. We introduced two sgRNAs targeted to exons 1 and 3 of *PHEX*, respectively, into 610B1 iPSCs together with the recombinant Cas9 protein. In *PHEX*-KO clone #1 iPSCs, a deletion extending from

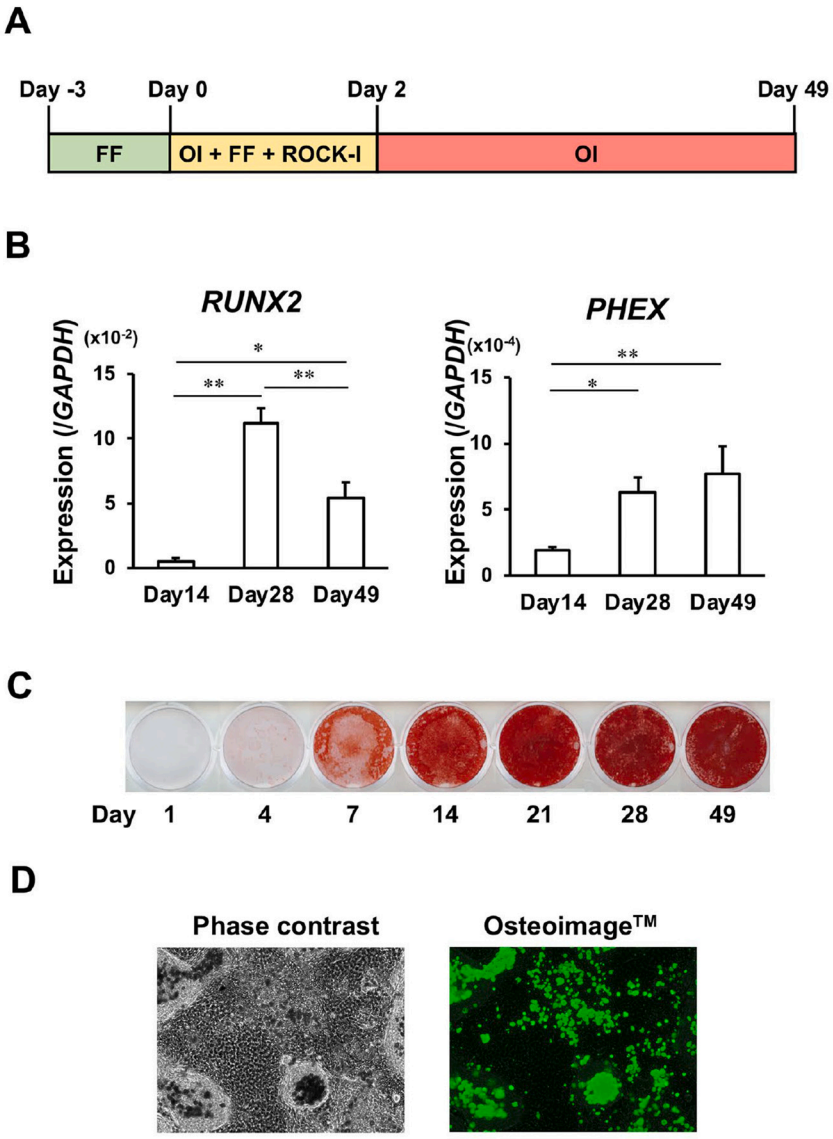

Fig. 1. Induction of *PHEX* expression during differentiation into the osteoblast lineage in control iPSCs derived from a healthy male.
(A) Schematic overview of the protocol for the osteogenic induction of human iPSCs. Cells were plated on Day 0 in the mixture of 20 % feeder-free (FF) medium and 80 % osteogenic induction (OI) medium containing a ROCK inhibitor. Two days later, the medium was replaced with 100 % OI medium, and cells were cultured for up to 49 days. (B) Real-time PCR for the expression of *RUNX2* and *PHEX* during the osteogenic differentiation of the human iPSC line 610B1 derived from a healthy male. The copy number of the target cDNA was estimated by referring to a standard curve and was normalized based on that of *GAPDH*. Data are shown as the mean ± SD ($n = 3$). *, $p < 0.05$ and **, $p < 0.01$. (C) Alizarin red staining of 610B1 iPSCs after osteogenic induction for the indicated periods. (D) Fluorescence image of OsteoImage™-stained hydroxyapatite accumulation and phase contrast image of the same region of the culture of 610B1 iPSCs on Day 21.

exon 1 to exon 3 resulted in a frameshift, creating a truncated protein consisting of 35 amino acids (c.95-254del, p.Leu33MetfsTer4) (Fig. 2A). Since the WT PHEX protein consists of 749 amino acids, the truncated protein with only 35 amino acids is assumed to be non-functional. Genomic PCR using the primer pair Ex1a-F and Int1-R amplified a 714-bp fragment only in the control 610B1 iPSCs isogenic except for *PHEX*. On the other hand, genomic PCR using the primer pair Ex1a-F and Int3-R amplified a 696-bp fragment in *PHEX*-KO #1 iPSCs, while no products were detected in isogenic control 610B1 iPSCs, which may have been due to the presence of long introns (Fig. 2B). We then induced the osteoblastic differentiation of *PHEX*-KO #1 iPSCs and isogenic control 610B1 iPSCs by following the protocol shown in Fig. 1A, and extracted RNA on Day 49 to examine the expression of *PHEX* transcripts. As expected, RT-PCR using the primer pair Ex1b-F and Ex5-R amplified 684-bp and 524-bp fragments in osteoblast lineage cells differentiated from control iPSCs and those from *PHEX*-KO #1 iPSCs, respectively. In addition, RT-PCR using the primer pair Ex2-F and Ex3-R produced a 116-bp fragment in osteoblast lineage cells differentiated from control iPSCs, while no products were detected in those from *PHEX*-KO #1 iPSCs (Fig. 2C). We also performed real-time RT-PCR using the primer pair Ex2-F and Ex3-R and verified that the product was not detectable in osteoblast lineage cells from *PHEX*-KO #1 iPSCs (Fig. 2D). These results confirmed that osteoblast lineage cells differentiated from *PHEX*-KO #1 iPSCs lost the functional transcripts of the *PHEX* gene. We then collected 72-hour conditioned media from *PHEX*-KO #1 and isogenic control iPSCs after osteogenic induction for 49 days and measured intact FGF23. The levels of FGF23 produced were significantly higher in osteoblast lineage cells differentiated from *PHEX*-KO #1 iPSCs than in those from control iPSCs (Fig. 2D).

In consideration of the possibility of clonal differences, we also

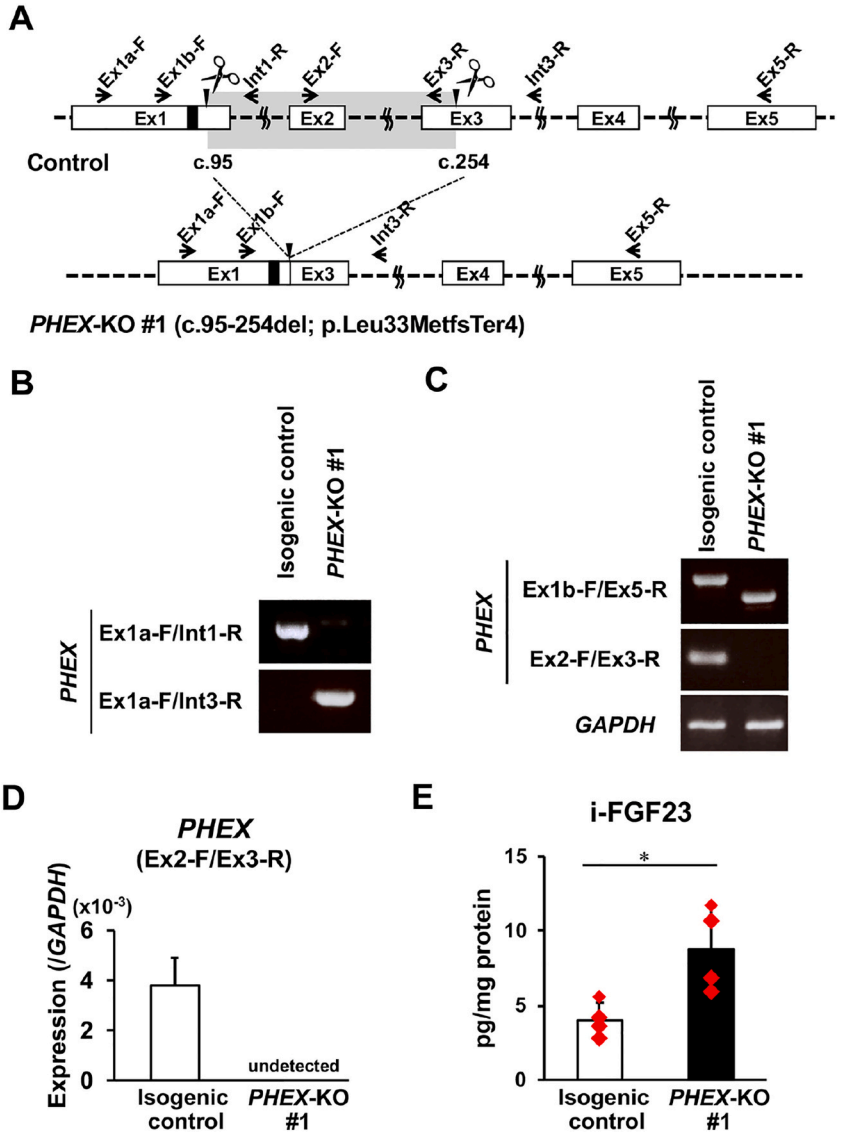

Fig. 2. Generation of *PHEX*-KO iPSCs.
(A) Schematic representation of the CRISPR/Cas9-mediated gene ablation of *PHEX*. The white boxes represent exons, and the black boxes indicate initiation codons. The arrowheads and scissors show the positions of target sequences for sgRNAs. The arrows represent the primers for PCR and their direction. In the *PHEX*-KO #1 clone, a deletion extending from exon 1 to exon 3 resulted in a frameshift, creating a truncated protein consisting of 35 amino acids (c.95-254del, p.Leu33MetfsTer4). (B) Genomic PCR using the indicated primer pairs and genomic DNA extracted from *PHEX*-KO #1 and isogenic control iPSCs. (C) RT-PCR using the indicated primer pairs and RNA extracted on Day 49 of the osteogenic induction of *PHEX*-KO #1 and isogenic control iPSCs. (D) SYBR Green-based real-time PCR using RNA extracted on Day 49 of osteogenic induction and the primer pair Ex2-F and Ex3-R. (E) Overproduction of FGF23 in osteoblast lineage cells derived from *PHEX*-KO #1 iPSCs. After osteogenic induction for 49 days, 72-hour conditioned media were harvested for the measurement of intact FGF23 by ELISA. FGF23 amounts were normalized based on the protein content of cell lysates. Data are shown as the mean ± SD ($n = 4$). *, $p < 0.05$.

analyzed another *PHEX*-KO iPSC clone (designated as *PHEX*-KO #2 iPSCs) in addition to *PHEX*-KO #1 iPSCs in the present study. *PHEX*-KO #2 iPSCs were found to have a deletion extending from exon 1 to exon 3, creating a truncated protein consisting of 25 amino acids (c.76-254del, p.Phe26Ter).

3.3. Similar viability and cytotoxicity between PHEX-KO and isogenic control iPSCs

We then evaluated the cell viability and cytotoxicity of undifferentiated *PHEX*-KO #1, #2 and isogenic control iPSCs using the MultiTox-Fluor Multiplex Cytotoxicity Assay (Promega). In the comparison between *PHEX*-KO #1 and isogenic control iPSCs, the numbers of live cells and those of dead cells were both similar at all time points. Furthermore, no significant differences were observed in the AFC/R110 ratio, an index for the ratio of live cells to dead cells (Fig. 3). Similar results were obtained in the comparison between *PHEX*-KO #2 and isogenic control iPSCs (Supplemental Fig. S1). Therefore, *PHEX* deficiency appeared to have negligible impact on the viability and cytotoxicity of iPSCs.

3.4. Enhanced in vitro mineralization in osteoblast lineage cells differentiated from PHEX-KO iPSCs than in those from the isogenic control iPSCs

We then induced *PHEX*-KO and isogenic control iPSCs to differentiate into the osteoblast lineage using the protocol shown in Fig. 1A. Under these culture conditions, β-glycerophosphate was used as a donor of Pi. In Alizarin red staining, which detected calcium microcrystals, the positively stained area was significantly larger in the osteogenic culture of both *PHEX*-KO #1 and #2 iPSCs than in that of isogenic control iPSCs (Fig. 4A, B, Supplemental Fig. S2A). Therefore, we performed the OsteoImage™ Mineralization Assay (Lonza) to quantify the content of hydroxyapatite. Consistent with the results of Alizarin red staining, the hydroxyapatite content was higher in the osteogenic culture of *PHEX*-KO #1 and #2 iPSCs than in that of isogenic control iPSCs (Fig. 4C, D, Supplemental Fig. S2B). These results suggest that *PHEX*-deficient osteoblast lineage cells may have an increased capacity for mineralization under *in vitro* conditions with sufficient Pi, lacking the effects of the kidneys.

3.5. Increased levels of extracellular PPi and ATP and reduced TNSALP activity in osteoblast lineage cells derived from PHEX-KO iPSCs

Osteoblast lineage cells differentiated from both *PHEX*-KO #1 and #2 iPSCs showed more mineralization than those from isogenic control iPSCs. Since extracellular PPi inhibits the nucleation and growth of hydroxyapatite crystals, we measured extracellular PPi levels in the 72-hour conditioned media of *PHEX*-KO and isogenic control iPSCs harvested on Day 49 of osteogenic induction. The extracellular level of PPi was higher in osteoblast lineage cells differentiated from *PHEX*-KO #1 and #2 iPSCs than in those from isogenic control iPSCs (Fig. 5A, Supplemental Fig. S2D), which excluded the possibility that increased mineralization in the osteogenic culture of *PHEX*-KO iPSCs was caused by a decrease in extracellular PPi.

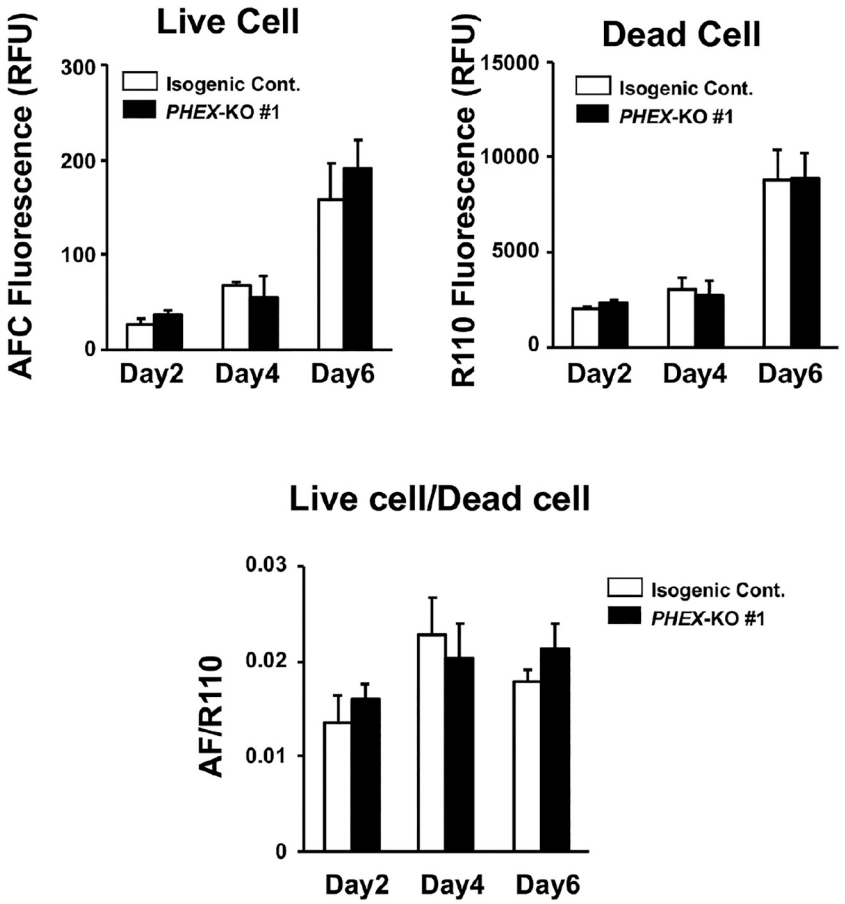

Fig. 3. Similar viability/cytotoxicity between *PHEX*-KO #1 and isogenic control iPSCs.
PHEX-KO #1 and isogenic control iPSCs were plated at 1×10^3 cells/well on 96-well plates and cultured for up to 6 days. The numbers of live cells and dead cells were determined at the indicated time points using a MultiTox-Fluor Multiplex Cytotoxicity Assay. The AFC/R110 ratio was calculated as an index for the ratio of live cells to dead cells. Data are shown as the mean ± SD (n = 4). No significant differences were observed in any parameters between *PHEX*-KO #1 and isogenic control iPSCs.

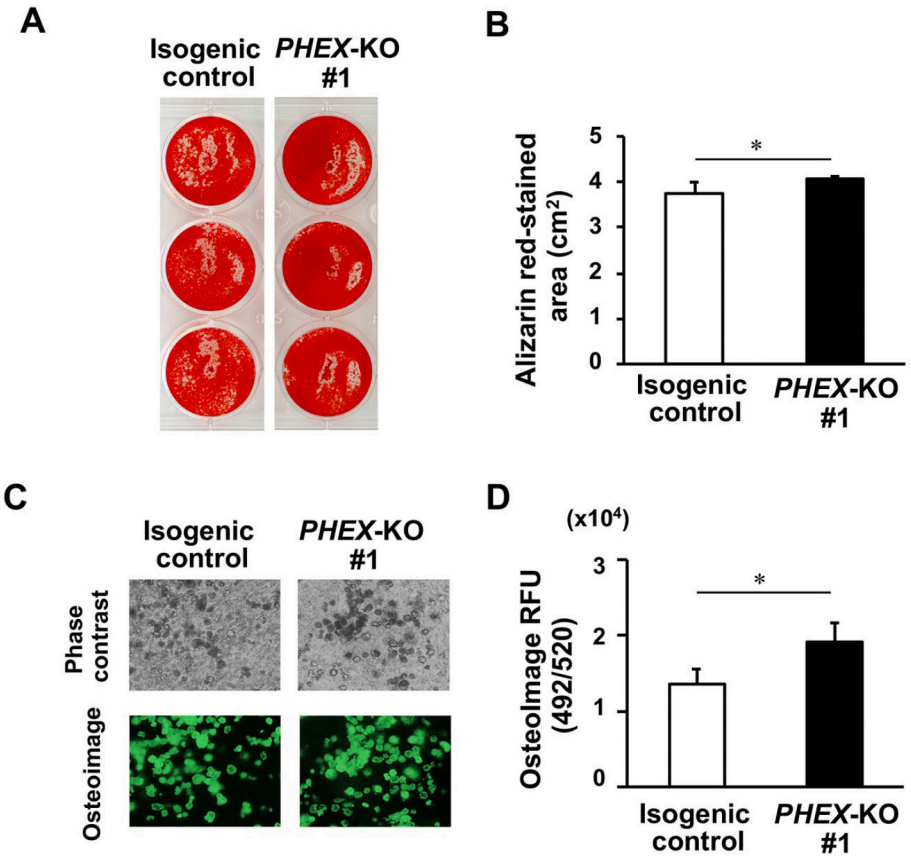

Fig. 4. Enhanced mineralization in osteoblast lineage cells derived from *PHEX*-KO #1 iPSCs compared to those from isogenic control iPSCs.
PHEX-KO #1 and the isogenic control iPSCs were plated at 4×10^5 cells/well on 12-well culture plates coated with iMatrix-511 silk and were induced to differentiate into osteoblast lineage cells. (A, B) Alizarin red staining assay on Day 49 of osteogenic induction. Quantification data of Alizarin red-stained areas are shown in (B). (C, D) Staining and quantification of hydroxyapatite by the OsteoImage™ assay on Day 49 of osteogenic induction. In (C), OsteoImage™-stained nodules and phase contrast images of the same field are shown. In (D), the hydroxyapatite content on Day 49 was quantified by reading stained plates on a fluorescence plate reader using 492 nm excitation and 520 nm emission wavelengths. Data in the graphs are shown as the mean ± SD ($n = 3$). *, $p < 0.05$.

We then examined the enzymatic activity of TNSALP, an ectoenzyme that hydrolyzes extracellular PPi to produce Pi. TNSALP enzymatic activity on Day 49 of osteogenic induction was lower in *PHEX*-KO #1 and #2 iPSCs than in control iPSCs (Fig. 5B, Supplemental Fig. S2C). Therefore, the elevated level of extracellular PPi in osteoblast lineage cells from *PHEX*-KO iPSCs may be partly explained by a reduction in TNSALP activity. The expression of the *ALPL* gene encoding TNSALP was lower in osteoblast lineage cells from *PHEX*-KO #2 iPSCs than in those from isogenic control iPSCs; however, the reduction was not significant in *PHEX*-KO #1 iPSCs (Fig. 5D, Supplemental Fig. S2F).

Since we and others previously reported that extracellular ATP also serves as a substrate for TNSALP [22,23], we examined ATP levels in conditioned media. Extracellular ATP levels were significantly elevated in osteoblast lineage cells from *PHEX*-KO #1 iPSCs, but not in those from *PHEX*-KO #2 iPSCs (Fig. 5C, Supplemental Fig. S2E).

In addition to TNSALP, ANKH and ectonucleotide pyrophosphatase/phosphodiesterase 1 (ENPP1) have been shown to play a role in the regulation of extracellular PPi levels. ANKH transports PPi from the intracellular to extracellular space, whereas ENPP1 hydrolyzes ATP to adenosine monophosphate (AMP) and PPi [24,25]. We assessed their expression levels in the osteogenic culture of *PHEX*-KO #1 iPSCs on Day 49 and found no significant difference from those in isogenic control iPSCs (Fig. 5E, F).

Since osteoblast lineage cells derived from *PHEX*-KO #1 and #2 iPSCs showed increased mineralization despite elevated levels of extracellular PPi, we also measured the concentration of extracellular Pi in 72-hour conditioned media harvested on Day 49 of osteogenic induction. Extracellular Pi levels were significantly higher in osteoblast lineage cells from *PHEX*-KO #1 iPSCs (Fig. 5G), but did not significantly differ between *PHEX*-KO #2 and isogenic control iPSCs (Supplemental Fig. S2G). Since the type III Na^+/Pi co-transporters PiT-1 and PiT-2 are involved in the regulation of extracellular Pi levels in osteoblastic cells [22], we examined their protein expression by Western blotting. The protein amount of PiT-1 was lower in osteoblast lineage cells differentiated from *PHEX*-KO #1 and #2 iPSCs than in those from control iPSCs (Fig. 5H, Supplemental Fig. S2H), which may have inhibited the uptake of Pi from the extracellular milieu. The amount of PiT-2 was similar between *PHEX*-KO and isogenic control cells (Fig. 5I, Supplemental Fig. S2I).

3.6. *Increased expression of Opn, Dmp1, Runx2, Fgfr1, and early growth response 1 (Egr1) in osteoblasts/osteocytes of Phex-deficient Hyp mice*

To date, the *Phex*-deficient *Hyp* mouse has markedly contributed to research on the pathogenesis of XLH. We previously reported that the expression of multiple genes, including *Dmp1*, canonical FGF ligands (*Fgf1* and *Fgf2*), and FGF receptors were up-regulated in the osteocytes of *Hyp* mice [8]. To confirm these findings and examine the expression of additional genes, we isolated osteoblasts and osteocytes from the femurs and tibiae of 12-week-old male *Hyp* ($Phex^{Hyp}/Y$) mice and WT littermates. Minced bones were subjected to sequential digestion with collagenase and decalcification with EGTA, and the cells released after each step were collected as fractions. Fresh cells of Fractions 3 to 5 and those of Fractions 6 to 9 were combined, and RNA was extracted for a

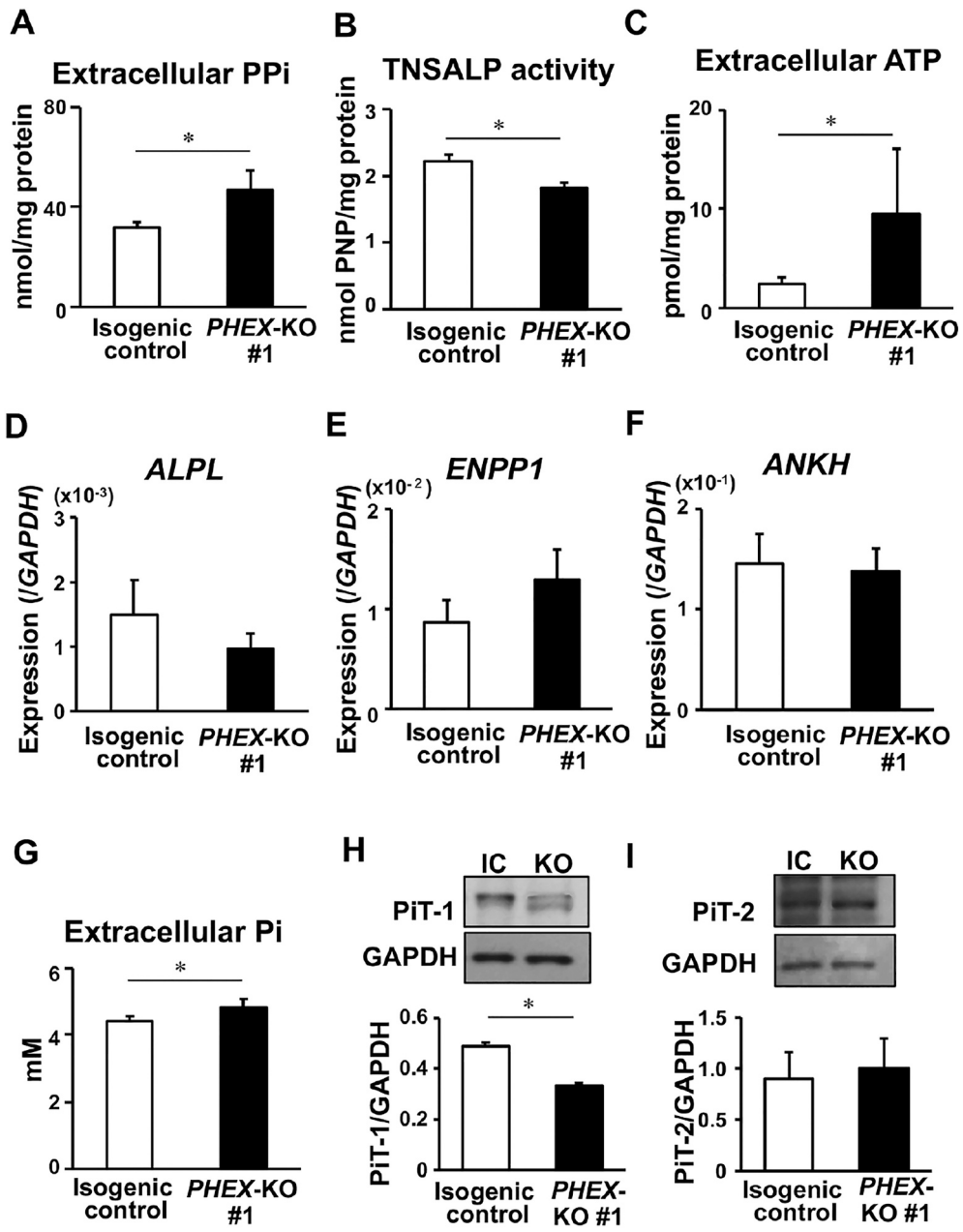

Fig. 5. Increased levels of extracellular PPi and ATP and reduced activity of TNSALP in osteoblast lineage cells derived from *PHEX*-KO #1 iPSCs. *PHEX*-KO #1 and isogenic control iPSCs were induced to differentiate into the osteoblast lineage for 49 days, and 72-hour conditioned media (CM) and cells were harvested. (A) Extracellular levels of PPi in CM. Values were normalized based on the protein content in cell lysates. (B) Enzymatic activity of TNSALP in cell lysates measured using *p*-nitrophenylphosphate as a substrate. (C) Extracellular levels of ATP in CM. Values were normalized based on the protein content in cell lysates. (D-F) The expression of *ALPL* (D), *ANKH* (E), and *ENPP1* (F) analyzed by real-time PCR. The copy number of target cDNA was normalized based on that of *GAPDH*. (G) Extracellular levels of Pi in CM. (H, I) The protein expression of type III Na^+/Pi co-transporters PiT-1 (H) and PiT-2 (I) analyzed by Western blotting. The results of densitometry are shown in the bottom graphs. Data in the graphs are shown as the mean ± SD (n = 3–6). *, $p < 0.05$.

real-time PCR analysis. We used Fractions 3–5 and Fractions 6–9 as osteoblast-rich and osteocyte-rich cells, respectively, based on our previous studies [8,20,21].

Consistent with our previous findings [8], the expression of *Kera* (an osteoblast marker), *Dmp1*, *Fgfr1*, *Fgf2*, and *early growth response 1* (*Egr1*), a downstream target for FGFR activation, was markedly higher in *Hyp* cells than in WT cells. In addition, the expression of *Runx2* and *Opn* (also known as *Spp1*) was higher in *Hyp* cells than in WT cells (Fig. 6), indicating that the expression of multiple genes was dysregulated in the osteoblast lineage cells of *Phex*-deficient *Hyp* mice.

3.7. Increased expression of OPN, DMP1, RUNX2, FGFR1 and EGR1 in osteoblast lineage cells derived from PHEX-KO iPSCs

We then investigated whether gene dysregulation similar to that found in the osteoblasts/osteocytes of *Hyp* mice was shared by the osteoblast lineage cells differentiated from human *PHEX*-KO iPSCs. We performed Western blotting to examine the protein expression of OPN and DMP1, both of which are members of the Small Integrin-Binding Ligand, N-linked Glycoprotein (SIBLING) family of extracellular matrix proteins. The protein expression of OPN was increased during the osteoblastic differentiation of control iPSCs, and peaked on Day 28 in *PHEX*-KO #1 iPSCs. At all time points, OPN protein expression was

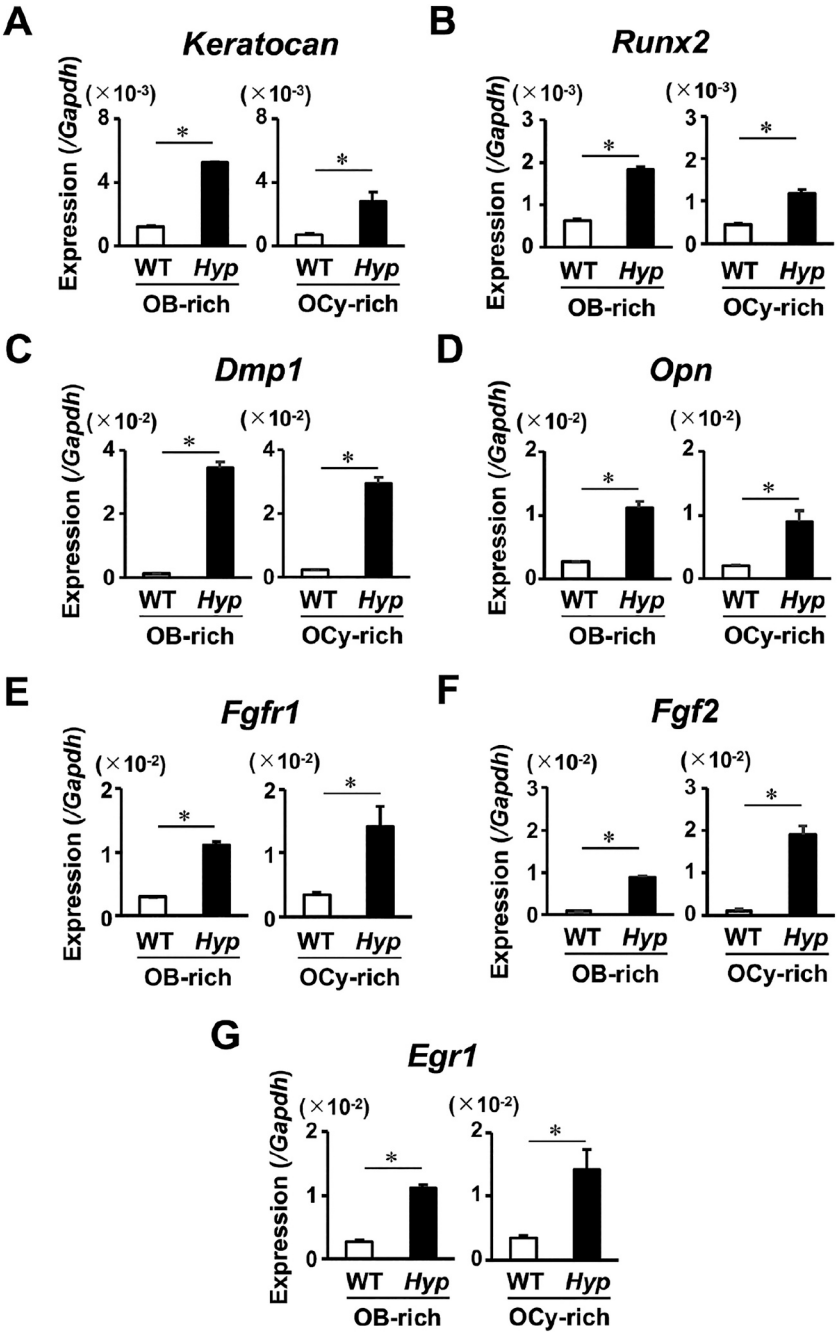

Fig. 6. Dysregulation of multiple genes in osteoblasts/osteocytes of *Phex*-deficient *Hyp* mice. Osteoblasts and osteocytes were isolated from the tibiae and femurs of 12-week-old male wild-type (WT) and *Hyp* mice by the sequential treatment of minced bones with collagenase and EGTA. RNA was extracted from the freshly isolated cells of osteoblast (OB)-rich fractions (Fractions 3–5) and osteocyte (OCy)-rich fractions (Fractions 6–9) and was subjected to real-time PCR for the indicated genes. Data are shown as the mean ± SD (n = 3). *, $p < 0.05$.

higher in osteoblast lineage cells from *PHEX*-KO #1 iPSCs than in those from isogenic control iPSCs (Fig. 7A). The expression of DMP1 was progressively increased by osteogenic induction in both *PHEX*-KO #1 and isogenic control iPSCs, and was markedly up-regulated in *PHEX*-KO #1 iPSCs (Fig. 7B). The increased protein expression of OPN and DMP1 was also confirmed in osteoblast lineage cells differentiated from *PHEX*-KO #2 iPSCs (Supplemental Fig. S3A, B).

In real-time PCR, the expression of *RUNX2, OPN, FGFR1* and *EGR1* was higher at most of the time points examined in osteoblast lineage cells from both *PHEX*-KO #1 and #2 iPSCs than in those from control iPSCs (Fig. 7C, Supplemental Fig. S3C). Since *EGR1* is a target gene of FGFR signaling, its up-regulation suggests the enhanced activation of FGFR signaling in osteoblast lineage cells derived from *PHEX*-KO iPSCs. The expression of *FGF2*, which was also up-regulated in *Hyp* osteoblasts/osteocytes, was similar between osteoblast lineage cells from *PHEX*-KO #1 and those from control iPSCs. The expression of *KLOTHO*, which encodes a co-receptor for FGF23, was also assessed in osteoblast lineage cells from *PHEX*-KO #1 and control iPSCs, and was found to be very low (Fig. 7C).

3.8. Enhanced CREB phosphorylation and increased PTHRP expression in osteoblast lineage cells derived from PHEX-KO iPSCs

We next investigated the impact of the deletion of *PHEX* on signaling

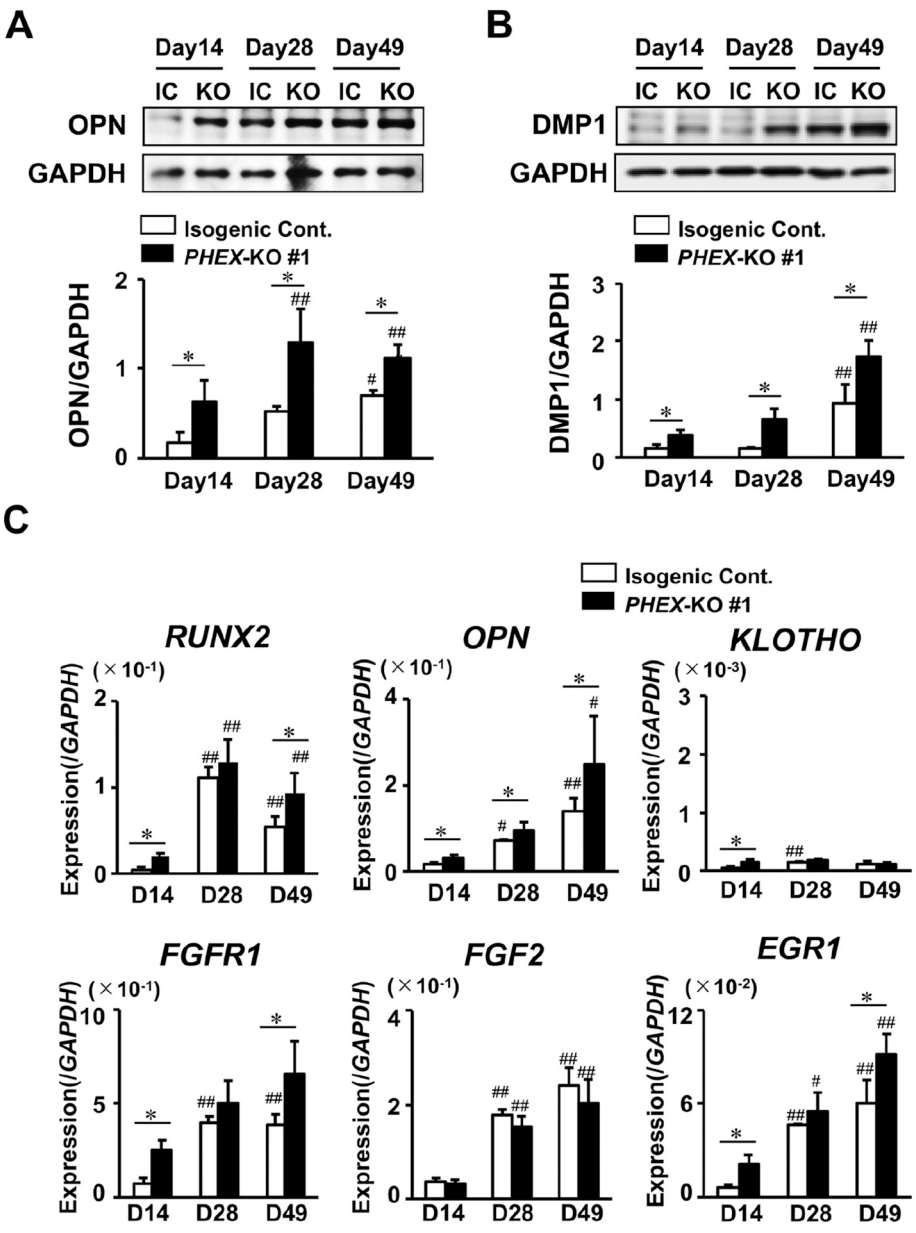

Fig. 7. Up-regulation of SIBLING proteins, *RUNX2*, *FGFR1*, and *EGR1* in osteoblast lineage cells derived from *PHEX*-KO #1 iPSCs.
PHEX-KO #1 and isogenic control iPSCs were induced to differentiate into the osteoblast lineage and were harvested at the indicated time points. (A, B) Western blotting was performed to examine the protein expression of the SIBLING proteins OPN (A) and DMP1 (B). The membranes were re-probed with an anti-GAPDH antibody, and densitometry was performed (bottom panels). (C) Real-time PCR was conducted to analyze the expression of the indicated genes. Data in the graphs are shown as the mean ± SD (n = 3). $^{\#}$, $P < 0.05$; $^{\#\#}$, $P < 0.01$ *vs* Day 14. *, $p < 0.05$.

pathways involved in osteoblastic differentiation. *PHEX*-KO iPSCs and isogenic controls cells were subjected to osteogenic induction, and cell lysates were harvested for Western blotting on Days 14, 28, and 49.

Since the expression of *FGFR1* and *EGR1* was up-regulated in osteoblast lineage cells derived from *PHEX*-KO #1 and #2 iPSCs (Fig. 7C, Supplemental Fig. S3C), we examined the phosphorylation status of FRS2α, an adaptor protein for FGFRs. The phosphorylation of FRS2α at Tyr 196 appeared to be stronger in osteoblast lineage cells from *PHEX*-KO iPSCs than in those from isogenic control iPSCs on Day 49 (Fig. 8A, Supplemental Fig. S4A). The phosphorylation of extracellular signal-regulated kinase (ERK) 1/2 was increased in osteoblast lineage cells from *PHEX*-KO #1 and #2 iPSCs on Days 28 and 49 (Fig. 8B, Supplemental Fig. S4B).

We also found the increased phosphorylation of cyclic AMP response element binding protein (CREB) at Ser133 in the osteoblast lineage cells derived from both *PHEX*-KO #1 and #2 iPSCs (Fig. 8C, Supplemental Fig. S4C). The phosphorylation of Smad 1 and Smad 5 at Ser463 and Ser465 was similar between *PHEX*-KO and isogenic control cells (Fig. 8D, Supplemental Fig. S4D).

Of note, the phosphorylation of CREB was markedly enhanced in osteoblast lineage cells derived from the *PHEX*-KO iPSCs. One of the major upstream molecules of the CREB pathway in osteoblast lineage cells is PTH type 1 receptor (PTH1R) for parathyroid hormone (PTH) and PTH-related protein (PTHrP), which is also called PTH-like hormone (PTHLH) [26,27]. Since our osteogenic culture of iPSCs was independent of the effects of the parathyroid, we examined the expression of *PTHRP* (*PTHLH*) and found its up-regulation in osteoblast lineage cells from *PHEX*-KO #1 and #2 iPSCs (Fig. 8E, Supplemental Fig. S4E). We also confirmed that the expression of *Pthrp* was increased in osteoblasts and osteocytes isolated from *Hyp* mice (Fig. 8F).

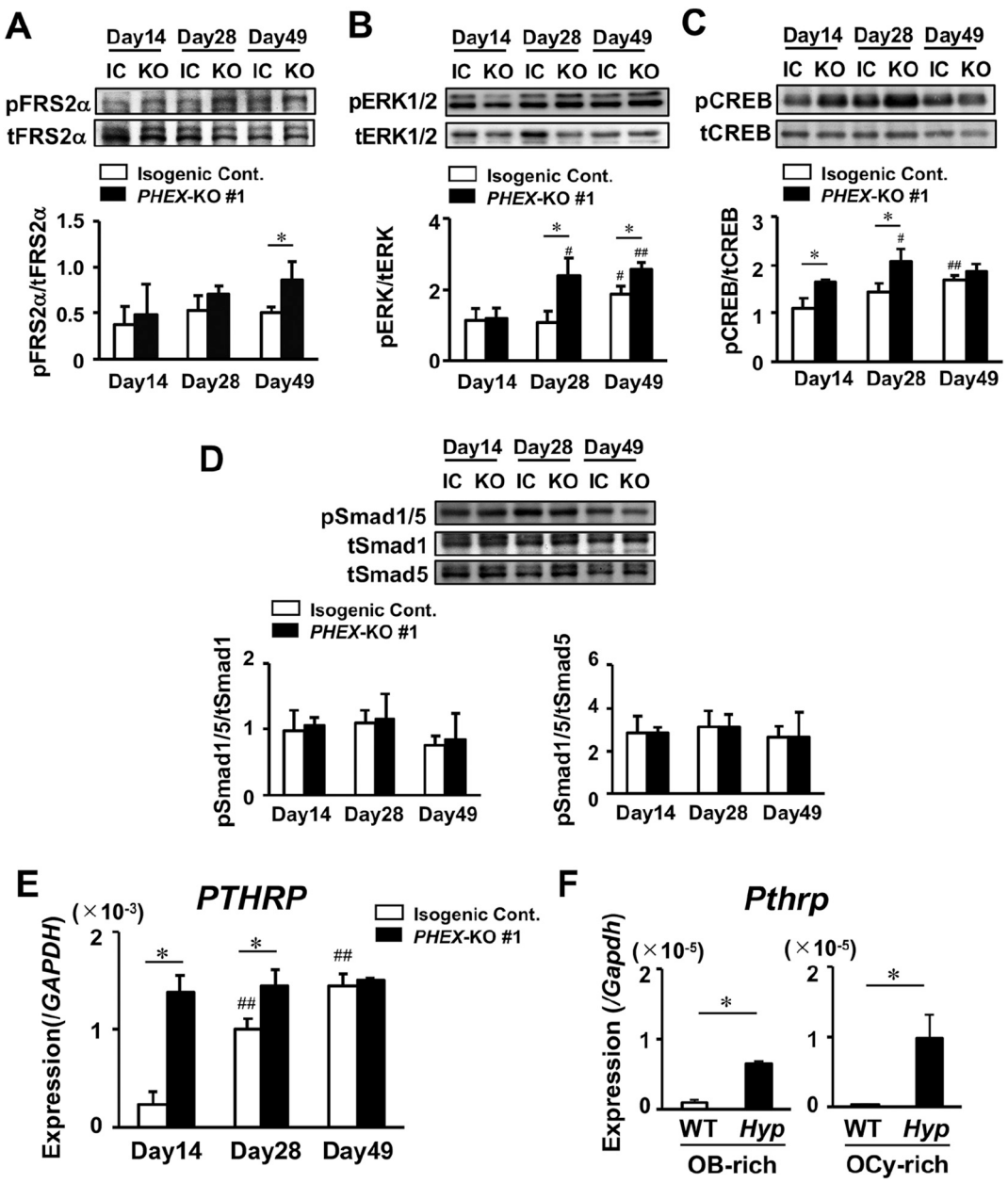

Fig. 8. Enhanced phosphorylation of CREB and increased expression of *PTHRP* in osteoblast lineage cells differentiated from *PHEX*-KO #1 iPSCs.
(A-D) *PHEX*-KO #1 and isogenic control iPSCs were induced to differentiate into the osteoblast lineage, and cells were harvested at the indicated time points to examine the phosphorylation of FRS2α at Tyr196 (A), ERK1/2 at Tyr180/Tyr182 (B), CREB at Ser133 (C), and Smad1 and Smad5 at Ser463 and Ser465 (D) by Western blotting. The results of densitometry are shown in the bottom graphs. (E) Real-time PCR for the expression of *PTHRP* in osteoblast lineage cells derived from *PHEX*-KO #1 and isogenic control iPSCs. (F) The expression of *Pthrp* in osteoblast (OB)-rich and osteocyte (OCy)-rich cells isolated from WT and *Hyp* mice. Data in graphs are shown as the mean ± SD (n = 3). $^{\#}$, $P < 0.05$; $^{\#\#}$, $P < 0.01$ *vs* Day 14. *, $p < 0.05$.

3.9. Effects of PHEX deficiency on gene responses to extracellular Pi in osteoblast lineage cells derived from iPSCs

Previous studies have suggested that an elevation of extracellular Pi evokes signal transduction to regulate gene expression, and the process may involve FGFR and type III Na^{+}/Pi co-transporters [20,28–30]. Since the expression of FGFR1 and PiT-1 was affected in osteoblast lineage cells derived from *PHEX*-KO iPSCs, responses to extracellular Pi might be altered in these cells. Therefore, we also examined the effects of *PHEX* deficiency on gene responses to changes in extracellular Pi levels in osteoblast lineage cells differentiated from the iPSCs. *PHEX*-KO and isogenic control iPSCs were induced to differentiate to osteoblast lineage cells for 42 days in the presence of β-glycerophosphate as described in Materials and Methods Section 2.4. The medium was then changed to Pi-free αMEM (Research Institute for the Functional Peptides, Yamagata, Japan) supplemented with 20 % FBS and 1 or 4 mM Pi instead of β-glycerophosphate, and cells were cultured for an additional 1 week (up to Day 49) before they were harvested. We performed real-time PCR to analyze the expression of *ALPL*, *OPN*, *FGFR1* and *EGR1*, the murine orthologues of which were previously reported to be regulated by Pi *in vitro* [21,30,31].

In osteoblast lineage cells derived from control iPSCs, the expression of *ALPL* was lower in the presence of 4 mM Pi than in the presence of 1 mM Pi. On the other hand, in osteoblast linage cells differentiated from *PHEX*-KO #1 and #2 iPSCs, no significant differences were observed in *ALPL* expression between 1 and 4 mM Pi (Fig. 9A、Supplemental

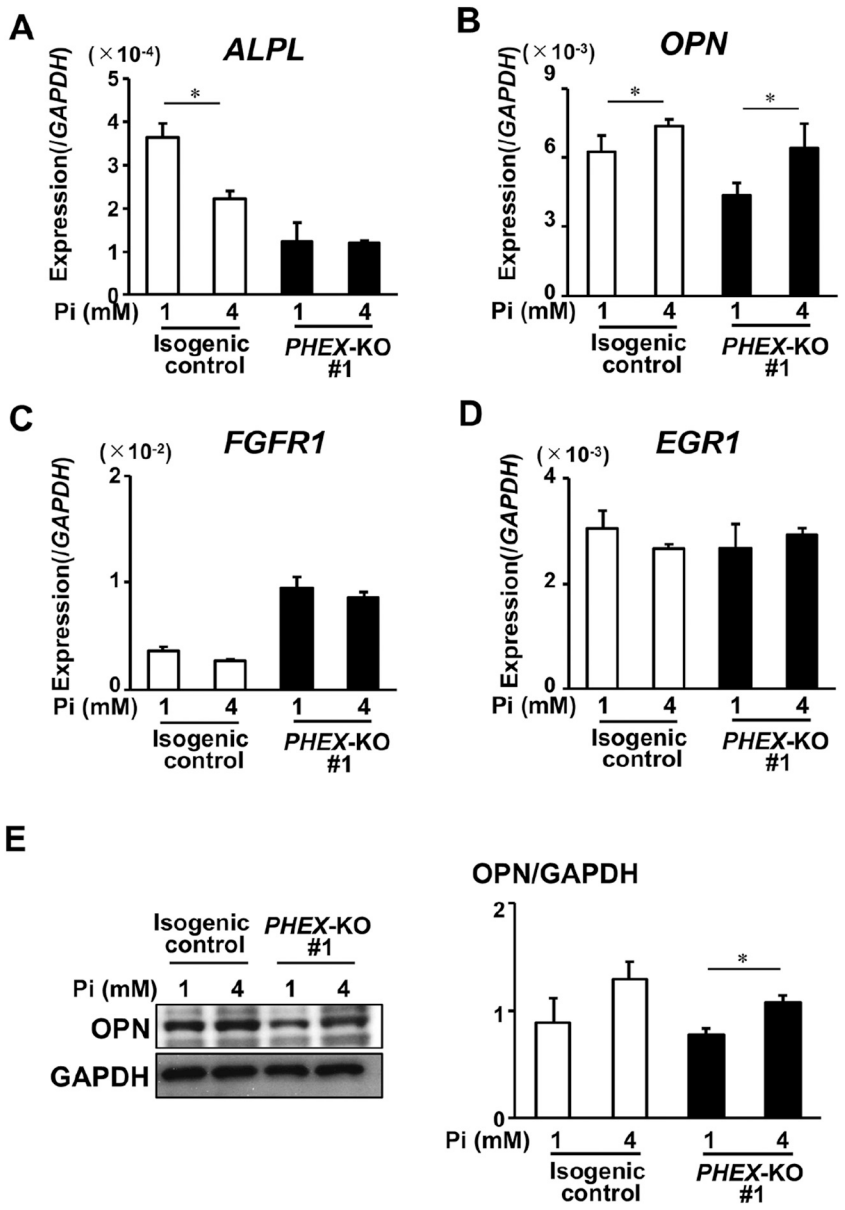

Fig. 9. Comparison of gene responses to extracellular Pi between osteoblast lineage cells derived from *PHEX*-KO #1 iPSCs and those from isogenic control iPSCs. *PHEX*-KO #1 and isogenic control iPSCs were induced to differentiate into the osteoblast lineage. On Day 42, the OI medium was changed to media containing 1 or 4 mM Pi instead of β-glycerophosphate, and cells were cultured for an additional 7 days. On Day 49, cells were harvested for real-time PCR (A-D) and Western blotting (E) to examine the expression of the indicated molecules. In (E), the results of densitometry are shown in the right panel. Data are shown as the mean ± SD (n = 3). *, $p < 0.05$.

Fig. S5A). The expression of *OPN* was slightly higher in the presence of 4 mM Pi in osteoblast lineage cells from both control iPSCs and *PHEX*-KO iPSCs (Fig. 9B, Supplemental Fig. S5B, E). No obvious differences were noted in the expression of *FGFR1* and *EGR1* between the 7-day treatment with 1 mM Pi and that with 4 mM Pi in both *PHEX*-KO and isogenic control iPSCs (Fig. 9C, D, Supplemental Fig. S5C, D).

4. Discussion

Accumulating evidence has suggested that mature osteoblasts and osteocytes play central roles in Pi homeostasis [13,32,33]. These cells express multiple molecules involved in Pi metabolism, which include FGF23, PHEX and DMP1. The FGF23-mediated bone-kidney axis reduces serum levels of Pi by increasing renal Pi excretion and decreasing the levels of $1,25(OH)_2D$. Inactivation of the *PHEX* gene causes XLH, which is the prototypic hypophosphatemic rickets/osteomalacia characterized by renal Pi wasting, hypophosphatemia, and reduced levels of serum $1,25(OH)_2D$ [1,2]. The administration of oral phosphate salts and active vitamin D metabolites has been a conventional medical treatment for the correction of hypophosphatemia and insufficient levels of serum $1,25(OH)_2D$, [1,2]. Since the overproduction of FGF23 in bone is responsible for renal Pi wasting, hypophosphatemia, and impaired vitamin D metabolism in XLH, the anti-FGF23 antibody burosumab has been developed to treat XLH patients [34–37]. In addition to hypophosphatemic rickets/osteomalacia, patients with XLH may also have a disproportionately short stature and dental abscess formation. Adult patients often develop complications such as osteoarthritis and enthesopathies [1,2,38]. Therefore, clinical manifestations in patients with XLH are complex. Mechanisms other than the overproduction of FGF23 also appear to be involved in the pathogenesis of XLH because previous mouse studies suggested that *Phex*-deficient osteoblast lineage cells have complex abnormalities [8,14,15]. However, among the findings

obtained from mouse models, it remains unclear which may be applied to human XLH. For example, the extent of elevations in serum FGF23 levels differ between *Phex*-deficient *Hyp* mice and human patients with XLH; they are higher than 1000 pg/mL in *Hyp* mice, but <100 pg/mL in the majority of XLH patients [6,8,39].

A more detailed understanding of the precise mechanisms underlying the pathogenesis of human XLH has been hindered partly due to the difficulties associated with obtaining sufficient osteoblasts and osteocytes for analyses from human subjects. Therefore, we herein generated *PHEX*-deficient human iPSCs and induced them to differentiate into the osteoblast lineage for use as a cell model of osteoblasts/osteocytes in human XLH. After confirming that control 610B1 iPSCs derived from a healthy male acquired the expression of *RUNX2* and *PHEX* when cultured in osteogenic medium (Fig. 1B, C), we applied CRISPR/Cas9-mediated genome editing to these cells and generated *PHEX*-KO iPSCs. This approach has enabled us to compare characteristics between osteoblast lineage cells derived from *PHEX*-KO iPSCs and those from control iPSCs isogenic except for the *PHEX* gene.

In the present study, we used an osteogenic medium containing β-glycerophosphate as a donor of Pi, based on a previous study [18]. To clarify the intrinsic abnormalities of *PHEX*-deficient osteoblast lineage cells independent of the effects of hypophosphatemia caused by the FGF23-mediated bone-kidney axis, we cultured *PHEX*-KO and isogenic control iPSCs using the same osteogenic medium containing 10 mM β-glycerophosphate. *In vitro* mineralization under these culture conditions was significantly greater in the osteogenic culture of *PHEX*-KO #1 and #2 iPSCs than in that of isogenic control iPSCs in both the Alizarin red staining assay and OsteoImage™ hydroxyapatite quantification assay (Fig. 4, Supplemental Fig. S2A, B). These results suggest that *PHEX*-deficient osteoblast lineage cells have an increased capacity to be mineralized in the presence of sufficient extracellular Pi. Interestingly, we found that the concentration of Pi in 72-hour conditioned media was higher in osteoblast lineage cells from *PHEX*-KO #1 iPSCs than in those from isogenic control iPSCs (Fig. 5G), which may have facilitated the propagation of hydroxyapatite and increased mineralization. We previously demonstrated that the CRISPR/Cas9-mediated gene ablation of Pit1 or Pit2 in the murine osteoblastic cell line MC3T3-E1 increased extracellular Pi levels by reducing its uptake into cells, which led to accelerated mineralization [22]. In the present study, the protein amount of PiT-1 was decreased in the osteoblast lineage cells derived from *PHEX*-KO #1 iPSCs (Fig. 5H), which may be involved in the increase observed in extracellular Pi. The decrease in the amount of PiT-1 was also confirmed in osteoblast lineage cells derived from *PHEX*-KO #2 iPSCs (Supplemental Fig. S2H); however, the increased level of extracellular Pi was not detected (Supplemental Fig. S2G), which may have been due to the rapid incorporation of extracellular free Pi into growing hydroxyapatite.

The accelerated mineralization in the osteogenic culture of *PHEX*-KO iPSCs reminded us of high bone mineral density and enthesopathy, a frequent complication in patients with XLH [38]. Clinical studies demonstrated that bone mineral apparent density of the lumber spine was elevated in children and adults with XLH compared to the reference groups, regardless of extra-skeletal calcifications [40,41]. Enthesopathy starts with the ectopic calcification of tendons and ligaments, and progressively forms osteophytes. It often affects spinal ligaments leading to spinal stenosis. Based on the current data, we speculate that increased Pi levels in the local extracellular microenvironment due to the dysregulation of PiT-1 might be involved in the high bone mass and enthesopathy in XLH. Conventional medical treatment for XLH using oral phosphate salts and active vitamin D neither prevented nor ameliorated enthesopathies [38]. The effects of burosumab on the prevention or treatment of enthesopathies have yet to be clarified.

Skeletal mineralization has been considered to be regulated mainly by the balance between extracellular Pi and PPi levels [42]. Extracellular Pi binds to calcium ions to produce calcium-phosphate crystals of hydroxyapatite, which accumulate and propagate on collagen fibrils in the extracellular matrix of bone. On the other hand, PPi inhibits mineralization by preventing the formation and growth of hydroxyapatite. TNSALP is an ectoenzyme that is present on the plasma membrane of osteoblast lineage cells and facilitates skeletal mineralization by degrading substrates such as PPi to generate Pi [42]. In the present study, we found that extracellular levels of PPi were increased in osteoblast lineage cells from *PHEX*-KO iPSCs, which excluded the possibility that accelerated mineralization was caused by reduction in extracellular PPi (Fig. 5A, Supplemental Fig. S2D). This increase in extracellular PPi appeared to be associated with a reduction in the activity of TNSALP (Fig. 5B, Supplemental Fig. S2C). The expression of *ENPP1* and *ANKH*, genes that encode other regulators of the extracellular levels of PPi, was not significantly affected by *PHEX* deficiency (Fig. 5E, F). Consistent with the present results, Murali et al. previously reported a decrease in the expression of *Alpl* encoding TNSALP and the accumulation of PPi in the bones of *Hyp* mice and in their osteocytes [43]. They also found that FGF23 suppressed the transcription of the *Alpl* gene *via* FGFR3 signaling [44]. More recently, a spatial metabolomics study demonstrated the up-regulation of several PPi-producing pathways in the cortical bone of *Hyp* mice [45]. These findings together with the present results suggest that *PHEX/Phex* deficiency induces the accumulation of extracellular PPi in both humans and mice.

We and others previously reported that extracellular ATP also serves as a substrate for TNSALP [22,23]. In parallel with this finding, reduced TNSALP activity in osteoblast lineage cells from *PHEX*-KO #1 iPSCs was associated with elevated levels of extracellular ATP (Fig. 5D); however, no significant difference was observed in extracellular ATP levels between the osteogenic culture of *PHEX*-KO #2 iPSCs and that of isogenic control iPSCs (Supplemental Fig. S2E), suggesting the complexity of the regulation of extracellular ATP levels.

The present study revealed that *PHEX/Phex* deficiency in osteoblast lineage cells caused the dysregulation of multiple genes, which was similar between humans and mice (Figs. 6, 7 and Supplemental Fig. S3). We found the up-regulation of *OPN/Opn*, also known as *SPP1/Spp1*, in both osteoblast lineage cells differentiated from *PHEX*-KO iPSCs and the osteoblasts/osteocytes of *Phex*-deficient *Hyp* mice. OPN and other SIBLINGs proteins, such as matrix extracellular phosphoglycoprotein (MEPE) and DMP1, share the acidic serine-aspartate rich MEPE-associated motif (ASARM) [14,46]. Full-length OPN and OPN-derived ASARM peptides may both function as inhibitors of mineralization [47]. A previous study demonstrated that the recombinant OPN protein was degraded by PHEX in *in vitro* cleavage assays, and OPN fragments accumulated in the bones of *Hyp* mice [14]. Since the deletion of the *Opn* gene partially restored the skeletal phenotype of *Hyp* mice without affecting the serum levels of Pi [15], the accumulation of OPN appears to contribute to the pathogenesis of *Hyp* mice. It is important to note that the present results revealed the mRNA expression of *OPN/Opn* increased as well as its protein amounts in osteoblast lineage cells derived from *PHEX*-KO iPSCs and the osteoblasts/osteocytes of *Hyp* mice (Figs. 6, 7B and Supplemental Fig. S3C). Therefore, PHEX may suppress the mRNA expression of *OPN/Opn*; however, this effect may be indirect. Beck, et al. previously reported that extracellular Pi triggered signal transduction in osteoblastic MC3T2-E1 cells to induce *Opn* expression [31,48]. Therefore, the up-regulation of *OPN* expression in osteoblast lineage cells derived from *PHEX*-KO iPSCs may be related to the altered availability of extracellular Pi. In addition, since Runx2 is known to transactivate the *Opn* gene [49], the increased expression of *RUNX2/Runx2* (Figs. 6B, 7C and Supplemental Fig. S3C) also may have contributed to the up-regulation of *OPN/Opn* in *PHEX/Phex* deficiency.

The expression of DMP1/Dmp1 was also increased in osteoblast lineage cells differentiated from *PHEX*-KO iPSCs and the osteoblasts/osteocytes of *Hyp* mice (Figs. 6, 7 and Supplemental Fig. S3). Since DMP1/Dmp1 is a member of the SIBLINGs family as well as OPN/Opn, this result supports a close relationship between PHEX and SIBLINGs proteins.

The increased expression of *RUNX2/Runx2* in *PHEX/Phex*-deficient

osteoblast lineage cells (Figs. 6B, 7C and Supplemental Fig. S3C) may play an important role in the pathogenesis of XLH because RUNX2/Runx2 functions as a fundamental transcription factor for skeletal development and is essential for osteoblast differentiation and chondrocyte maturation [49]. Mouse studies have suggested that Runx2 induces the commitment of multipotent mesenchymal cells into the osteoblast lineage and promotes the differentiation of pre-osteoblasts through mutual regulation with other signaling pathways, such as FGF/FGFR, hedgehog, and Wnt. In differentiated osteoblasts, Runx2 transactivates the genes encoding extracellular matrix proteins, including *Col1a1*, *Col1a2*, *osteocalcin*, *Dmp1*, and *Opn* [49,50]. In consideration of the multiple functions of RUNX2/Runx2 in osteoblasts, its up-regulation may markedly contribute to the complex changes in *PHEX/Phex*-deficient osteoblast lineage cells.

The up-regulation of *RUNX2* may also be involved in the enhanced *in vitro* mineralization in osteoblast lineage cells differentiated from *PHEX*-KO iPSCs. Byers et al. demonstrated that the retrovirus-mediated overexpression of *Runx2* accelerated the mineralization in immature MC3T3-E1 cells [51]. In addition, Gersbach et al. reported that the overexpression of *Runx2* induced the transdifferentiation of primary skeletal myoblasts into a mineralizing osteoblastic phenotype [52].

Consistent with our previous findings [8], the expression of *Fgfr1*, *Fgf2*, and *Egr1* was up-regulated in the osteoblasts/osteocytes of *Hyp* mice (Fig. 6). We herein demonstrated that the expression of *FGFR1* and *EGR1* was also higher in osteoblast lineage cells differentiated from *PHEX*-KO #1 and #2 iPSCs than in those from isogenic control iPSCs (Fig. 7 and Supplemental Fig. S3C). In addition, the phosphorylation of FRS2α and ERK1/2 increased in osteoblast lineage cells differentiated from *PHEX*-KO iPSCs (Fig. 8A, B, Supplemental Fig. S4A, B). These results indicate that *PHEX/Phex* deficiency in osteoblast lineage cells enhanced FGFR signaling in both humans and mice. This is of interest because FGFR1 has been suggested to play a role in sensing Pi availability. Previous cell studies demonstrated that a treatment with high Pi affected gene expression through the activation of FGFR [20,29,30]. In the MC3T3-E1 osteoblastic cell line, a treatment with high Pi up-regulated the expression of Dmp1, which was abolished by a pre-treatment with an FGFR inhibitor [20]. In mice, a high Pi diet increased the skeletal expression of the *Galnt3* (*polypeptide N-acetylgalactosaminyltransferase 3*) gene through the activation of FGFR1, which led to increase in serum FGF23 levels [53]. Therefore, enhanced FGFR signaling in osteoblast lineage cells differentiated from *PHEX*-KO iPSCs and *Hyp* osteoblasts/osteocytes suggests the involvement of abnormal Pi sensing in the pathogenesis of XLH.

It is important to note that the phosphorylation of CREB at Ser133 was markedly increased in osteoblast lineage cells derived from *PHEX*-KO #1 and #2 iPSCs (Fig. 8C, Supplemental Fig. S4C). CREB belongs to the CREB/activating transcription factor (ATF) family of transcription factors and plays critical roles in the regulation of cell proliferation, differentiation, apoptosis, and survival in response to various external stimuli [54]. CREB is activated by GPCR-stimulating signals, such as PTH, through the PKA-mediated phosphorylation of Ser133 and transactivates osteogenic genes including bone sialoprotein and osteocalcin [55]. Previous studies demonstrated that the activation of cAMP/PKA/CREB pathway increased *RUNX2* expression in human mesenchymal stem cells [56] and bone marrow stromal cells [57]. Furthermore, ChIP-Atlas (https://chip-atlas.org), a data-mining suite powered by comprehensive integration of ChIP-seq data, suggests that *RUNX2* is one of the target genes of CREB1. The present results revealed the up-regulation of *RUNX2/Runx2* in osteoblast lineage cells derived from *PHEX*-KO iPSCs and *Hyp* osteoblasts/osteocytes, which appeared to affect multiple genes and cell behavior. According to ChIP-Atlas, the putative target genes of RUNX2 include *FGFR1*, *OPN*, and *DMP1*. Therefore, the enhanced phosphorylation of CREB during the osteoblast differentiation may also contribute to the pathogenesis of XLH, partly through the up-regulation of *RUNX2*.

The present results suggest that the increased expression of PTHRP plays a role in the enhanced phosphorylation of CREB in osteoblast lineage cells derived from *PHEX*-KO iPSCs. PTHrP as well as PTH act on bone cells through PTH1R and the cyclic AMP/protein kinase A/CREB pathway [26,27]. A previous study using osteoblast-specific *Pthrp*-KO mice generated using *Col1a1*-Cre revealed that osteoblast-derived PTHrP functioned as an endogenous bone anabolic factor that augmented bone formation [58]. More recently, Ansari et al. reported that the deletion of *Pthrp* in mature osteoblasts and osteocytes in mice using the *Dmp1*-Cre driver reduced trabecular bone volume and osteoblast numbers and impaired the strength of cortical bone, but did not affect osteoclast numbers [59]. Therefore, PTHrP derived from osteoblast lineage cells appears to function as an autocrine/paracrine regulator of bone formation. Using the osteocytic cell line IDG-SW5 and lactating mice on a low calcium diet, Jähn et al. suggested that osteocytes may acidify their microenvironment in response to treatment with PTHrP, and this acidification may lead to the removal of calcium from perilacunar/pericanalicular matrices [60]. Based on these findings, we speculate that the increased production of PTHrP by osteoblast lineage cells may contribute to the formation of hypomineralized periosteocytic lesions, a bone feature in XLH [61]. Boileau et al. demonstrated the 107–139-residue fragment of PTHrP was degraded by a recombinant soluble, secreted form of human PHEX protein [62], which suggested a relationship between PHEX and PTHrP. The mechanism by which *PHEX/Phex* deficiency caused the up-regulation of *PTHRP/Pthrp* needs to be clarified in future studies.

Previous studies suggested that FGFR1 and type III Na^+/Pi cotransporters have roles in the transduction of signals evoked by extracellular Pi and/or Pi sensing. Therefore, we speculated that osteoblast lineage cells derived from *PHEX*-KO cells with the dysregulated expression of FGFR1 and PiT-1 may affect gene responses to extracellular Pi. We herein examined the effects of a chronic treatment with different levels of extracellular Pi and found that the treatment with higher (4 mM) Pi down-regulated *ALPL* expression in osteoblast lineage cells from isogenic control iPSCs but not in those from *PHEX*-KO iPSCs (Fig. 9A, Supplemental Fig. S5A). This was interesting because our previous study using WT mice demonstrated that a chronic treatment with high Pi markedly suppressed *Alpl* expression in osteoblasts and osteocytes isolated from adult mice but not in cells from young mice [21]. Regarding *OPN* expression, it was slightly increased by the treatment with higher Pi in osteoblast lineage cells from both *PHEX*-KO and isogenic control iPSCs; however, its up-regulation was clearer in those from *PHEX*-KO iPSCs (Fig. 9B, E, Supplemental Fig. S5B). It is important to note that *OPN* expression was lower in *PHEX*-KO cells than in isogenic control cells under this experimental condition, which was different from the results obtained when cells were analyzed on Day 49 of the osteogenic culture using β-glycerophosphate as a Pi donor (Fig. 7, Supplemental Fig. S3). This difference suggests that the impact of the change from β-glycerophosphate to Pi in media was stronger in osteoblast lineage cells from *PHEX*-KO iPSCs than in those from isogenic control iPSCs. Although a 24-hour treatment with high Pi was previously shown to increase the expression of *Fgfr1* and *Egr1* in the murine osteoblastic cell line MC3T3-E1 cells [20], the expression of *FGFR1* and *EGR1* in the present study was not markedly affected by the 7-day treatment with different levels of Pi (Fig. 9C, D, Supplemental Fig. S5C, D). Further studies are needed to clarify how *PHEX* deficiency affects the response to and regulation of extracellular levels of Pi in osteoblast lineage cells.

Some previous studies analyzed primary cells obtained from patients with XLH. For example, it was reported that cultured dermal fibroblasts from XLH patients showed normal response to $1,25(OH)_2D$ [63]. Dental pulp stem cells derived from exfoliated deciduous teeth of XLH patients exhibited a higher expression of OPN, DMP1 and MEPE than those from control subjects when cultured in an osteogenic medium [64]. The *PHEX*-KO human iPSC model used in the current study will be a complement to these approaches using primary cells from XLH patients. The advantages of the iPSC model used here include the abundance of cells

and the availability of isogenic control cells.

There are also limitations in the current study. The increased mineralization in the osteoblast lineage cells derived from *PHEX*-KO iPSCs *in vitro* was different from the observation *in vivo* of XLH. Chronic hypophosphatemia in XLH causes Pi deficiency in the bone microenvironment, which impairs the formation and propagation of hydroxyapatite crystals. We found that the increased expression of *PTHRP/Pthrp, RUNX2/Runx2*, *DMP1/Dmp1*, *OPN/Opn*, *FGFR1/Fgfr1* and *EGR1/Egr1* was shared by both the osteoblast lineage cells differentiated from *PHEX*-KO iPSCs and the osteoblasts/osteocytes isolated from *Hyp* mice (Fig. 6, 7, 8E, F, Supplemental Fig. S3, S4F), which suggests that *PHEX/Phex* deficiency itself leads to the up-regulation of these genes independently of the extracellular Pi levels. However, since previous studies including ours demonstrated that treatment with high Pi increased the expression of *Dmp1*, *Opn*, *Fgfr1* and *Egr1* in MC3T3-E1 murine osteoblastic cell line [20,31], hypophosphatemia may influence the expression of these genes *in vivo*. The expression of *ALPL/Alpl* gene is usually suppressed by an elevation of extracellular Pi [21,30], and hypophosphatemia *in vivo* is likely to up-regulate the gene. Moreover, impaired skeletal mineralization *in vivo* of XLH may affect the bone microenvironment, which in turn may influence environmental signals such as mechanical stress-induced signaling. Therefore, the pathogenic mechanisms at work *in vivo* of XLH may be more complex than those involved in the cell model used in the current study.

5. Conclusion

By utilizing *PHEX*-KO human iPSCs generated by CRISPR/Cas9-mediated gene ablation, we obtained evidence to show that complex intrinsic abnormalities in osteoblast lineage cells may contribute to the pathogenesis of human XLH. Osteoblast lineage cells differentiated from *PHEX*-KO iPSCs displayed enhanced mineralization than those from isogenic control iPSCs, suggesting that *PHEX*-deficient osteoblast lineage cells may have an increased mineralizing capacity under a sufficient supply of Pi. The levels of extracellular PPi were increased in osteoblast lineage cells differentiated from *PHEX*-KO iPSCs, which was partly due to the reduced activity of TNSALP. The protein amount of PiT-1 was decreased in osteoblast lineage cells differentiated from *PHEX*-KO iPSCs. *PHEX* deficiency also resulted in the dysregulation of multiple molecules, signaling pathways, and gene responses to extracellular Pi and in human iPSCs-derived osteoblast lineage cells. Enhanced CREB pathway associated with the up-regulation of *PTHRP* appeared to increase the expression of *RUNX2*, which might have affected the expression of various genes such as *OPN* and *DMP1* and capacity to be mineralized. These results provide insights into the pathophysiology of XLH and may contribute to the development of new therapeutic strategies for the disease.

CRediT authorship contribution statement

Tatsuro Nakanishi: Writing – review & editing, Writing – original draft, Visualization, Methodology, Investigation, Formal analysis. **Miwa Yamazaki:** Writing – review & editing, Methodology, Investigation, Formal analysis. **Kanako Tachikawa:** Writing – review & editing, Methodology, Investigation, Formal analysis. **Ayu Ueta:** Writing – review & editing, Investigation, Formal analysis. **Masanobu Kawai:** Writing – review & editing, Methodology. **Keiichi Ozono:** Writing – review & editing, Funding acquisition, Conceptualization. **Toshimi Michigami:** Writing – review & editing, Writing – original draft, Visualization, Investigation, Funding acquisition, Formal analysis, Data curation, Conceptualization.

Declaration of competing interest

TM received consultation fees from Kyowa-Kirin Co. Ltd. and lecture fees from Kyowa-Kirin Co. Ltd., and Alexion Pharma. KO received consultation fees from Kyowa-Kirin Co. Ltd. And lecture fees from Kyowa-Kirin Co. Ltd., Alexion Pharma and Pfizer.

Data availability

Data will be made available on request.

Acknowledgments

This work was supported in part by grants from the Japan Society for the Promotion of Science (JSPS KAKENHI Grant Numbers 18K07838 and 21K07835 to TM and 21H02881 to KO) and a grant from the Foundation for Growth Science (Grant Number 2022-8 to TM).

Appendix A. Supplementary data

Supplementary data to this article can be found online at https://doi.org/10.1016/j.bone.2024.117044.

References

[1] T.O. Carpenter, E.A. Imel, I.A. Holm, S.M. Jan de Beur, K.L. Insogna, A clinician's guide to X-linked hypophosphatemia, J. Bone Miner. Res. 26 (7) (2011) 1381–1388.
[2] D. Haffner, F. Emma, D.M. Eastwood, M.B. Duplan, J. Bacchetta, D. Schnabel, P. Wicart, D. Bockenhauer, F. Santos, E. Levtchenko, P. Harvengt, M. Kirchhoff, F. Di Rocco, C. Chaussain, M.L. Brandi, L. Savendahl, K. Briot, P. Kamenicky, L. Rejnmark, A. Linglart, Clinical practice recommendations for the diagnosis and management of X-linked hypophosphataemia, Nat. Rev. Nephrol. 15 (7) (2019) 435–455.
[3] M. Yamazaki, T. Michigami, Osteocytes and the pathogenesis of hypophosphatemic rickets, Front. Endocrinol. (Lausanne) 13 (2022) 1005189.
[4] T. Shimada, S. Mizutani, T. Muto, T. Yoneya, R. Hino, S. Takeda, Y. Takeuchi, T. Fujita, S. Fukumoto, T. Yamashita, Cloning and characterization of FGF23 as a causative factor of tumor-induced osteomalacia, Proc. Natl. Acad. Sci. U. S. A. 98 (11) (2001) 6500–6505.
[5] S. Sarafrazi, S.C. Daugherty, N. Miller, P. Boada, T.O. Carpenter, L. Chunn, K. Dill, M.J. Econs, S. Eisenbeis, E.A. Imel, B. Johnson, M.J. Kiel, S. Krolczyk, P. Ramesan, R. Truty, Y. Sabbagh, Novel PHEX gene locus-specific database: comprehensive characterization of vast number of variants associated with X-linked hypophosphatemia (XLH), Hum. Mutat. 43 (2) (2022) 143–157.
[6] Y. Ohata, Y. Ishihara, Pathogenic variants of the PHEX gene, Endocrines 3 (3) (2022) 498–511.
[7] B.R. Coyac, G. Falgayrac, B. Baroukh, L. Slimani, J. Sadoine, G. Penel, M. Biosse-Duplan, T. Schinke, A. Linglart, M.D. McKee, C. Chaussain, C. Bardet, Tissue-specific mineralization defects in the periodontium of the Hyp mouse model of X-linked hypophosphatemia, Bone 103 (2017) 334–346.
[8] K. Miyagawa, M. Yamazaki, M. Kawai, J. Nishino, T. Koshimizu, Y. Ohata, K. Tachikawa, Y. Mikuni-Takagaki, M. Kogo, K. Ozono, T. Michigami, Dysregulated gene expression in the primary osteoblasts and osteocytes isolated from hypophosphatemic Hyp mice, PLoS One 9 (4) (2014) e93840.
[9] M.K. Drezner, PHEX gene and hypophosphatemia, Kidney Int. 57 (1) (2000) 9–18.
[10] A. Benet-Pages, B. Lorenz-Depiereux, H. Zischka, K.E. White, M.J. Econs, T. M. Strom, FGF23 is processed by proprotein convertases but not by PHEX, Bone 35 (2) (2004) 455–462.
[11] L. Beck, Y. Soumounou, J. Martel, G. Krishnamurthy, C. Gauthier, C.G. Goodyer, H. S. Tenenhouse, Pex/PEX tissue distribution and evidence for a deletion in the 3' region of the Pex gene in X-linked hypophosphatemic mice, J. Clin. Invest. 99 (6) (1997) 1200–1209.
[12] S. Liu, W. Tang, J. Zhou, J.R. Stubbs, Q. Luo, M. Pi, L.D. Quarles, Fibroblast growth factor 23 is a counter-regulatory phosphaturic hormone for vitamin D, J. Am. Soc. Nephrol. 17 (5) (2006) 1305–1315.
[13] B. Yuan, M. Takaiwa, T.L. Clemens, J.Q. Feng, R. Kumar, P.S. Rowe, Y. Xie, M. K. Drezner, Aberrant Phex function in osteoblasts and osteocytes alone underlies murine X-linked hypophosphatemia, J. Clin. Invest. 118 (2) (2008) 722–734.
[14] N.M. Barros, B. Hoac, R.L. Neves, W.N. Addison, D.M. Assis, M. Murshed, A. K. Carmona, M.D. McKee, Proteolytic processing of osteopontin by PHEX and accumulation of osteopontin fragments in Hyp mouse bone, the murine model of X-linked hypophosphatemia, J. Bone Miner. Res. 28 (3) (2013) 688–699.
[15] B. Hoac, M. Ostergaard, N.K. Wittig, T. Boukpessi, D.J. Buss, C. Chaussain, H. Birkedal, M. Murshed, M.D. McKee, Genetic ablation of Osteopontin in Osteomalacic Hyp mice partially rescues the deficient mineralization without correcting hypophosphatemia, J. Bone Miner. Res. 35 (10) (2020) 2032–2048.
[16] A. Martin, S. Liu, V. David, H. Li, A. Karydis, J.Q. Feng, L.D. Quarles, Bone proteins PHEX and DMP1 regulate fibroblastic growth factor Fgf23 expression in osteocytes through a common pathway involving FGF receptor (FGFR) signaling, FASEB J. 25 (8) (2011) 2551–2562.
[17] Z. Xiao, J. Huang, L. Cao, Y. Liang, X. Han, L.D. Quarles, Osteocyte-specific deletion of Fgfr1 suppresses FGF23, PLoS One 9 (8) (2014) e104154.

[18] S. Kawai, H. Yoshitomi, J. Sunaga, C. Alev, S. Nagata, M. Nishio, M. Hada, Y. Koyama, M. Uemura, K. Sekiguchi, H. Maekawa, M. Ikeya, S. Tamaki, Y. Jin, Y. Harada, K. Fukiage, T. Adachi, S. Matsuda, J. Toguchida, In vitro bone-like nodules generated from patient-derived iPSCs recapitulate pathological bone phenotypes, Nat. Biomed. Eng. 3 (7) (2019) 558–570.
[19] K. Hino, M. Ikeya, K. Horigome, Y. Matsumoto, H. Ebise, M. Nishio, K. Sekiguchi, M. Shibata, S. Nagata, S. Matsuda, J. Toguchida, Neofunction of ACVR1 in fibrodysplasia ossificans progressiva, Proc. Natl. Acad. Sci. U. S. A. 112 (50) (2015) 15438–15443.
[20] J. Nishino, M. Yamazaki, M. Kawai, K. Tachikawa, K. Yamamoto, K. Miyagawa, M. Kogo, K. Ozono, T. Michigami, Extracellular phosphate induces the expression of dentin matrix protein 1 through the FGF receptor in osteoblasts, J. Cell. Biochem. 118 (5) (2017) 1151–1163.
[21] T. Michigami, K. Tachikawa, M. Yamazaki, T. Nakanishi, M. Kawai, K. Ozono, Growth-related skeletal changes and alterations in phosphate metabolism, Bone 161 (2022) 116430.
[22] M. Yamazaki, M. Kawai, S. Kinoshita, K. Tachikawa, T. Nakanishi, K. Ozono, T. Michigami, Clonal osteoblastic cell lines with CRISPR/Cas9-mediated ablation of Pit1 or Pit2 show enhanced mineralization despite reduced osteogenic gene expression, Bone 151 (2021) 116036.
[23] W. Liu, L. Zhang, K. Xuan, C. Hu, S. Liu, L. Liao, B. Li, F. Jin, S. Shi, Y. Jin, Alpl prevents bone ageing sensitivity by specifically regulating senescence and differentiation in mesenchymal stem cells, Bone Res. 6 (2018) 27.
[24] E. Mitton-Fitzgerald, C.M. Gohr, B. Bettendorf, A.K. Rosenthal, The role of ANK in calcium pyrophosphate deposition disease, Curr. Rheumatol. Rep. 18 (5) (2016) 25.
[25] F. Roberts, D. Zhu, C. Farquharson, V.E. Macrae, ENPP1 in the regulation of mineralization and beyond, Trends Biochem. Sci. 44 (7) (2019) 616–628.
[26] M.N. Wein, Parathyroid hormone signaling in osteocytes, JBMR Plus 2 (1) (2018) 22–30.
[27] T.J. Martin, PTH1R actions on bone using the cAMP/protein kinase a pathway, Front. Endocrinol. (Lausanne) 12 (2021) 833221.
[28] T. Michigami, M. Kawai, M. Yamazaki, K. Ozono, Phosphate as a signaling molecule and its sensing mechanism, Physiol. Rev. 98 (4) (2018) 2317–2348.
[29] M. Yamazaki, K. Ozono, T. Okada, K. Tachikawa, H. Kondou, Y. Ohata, T. Michigami, Both FGF23 and extracellular phosphate activate Raf/MEK/ERK pathway via FGF receptors in HEK293 cells, J. Cell. Biochem. 111 (5) (2010) 1210–1221.
[30] M. Kimata, T. Michigami, K. Tachikawa, T. Okada, T. Koshimizu, M. Yamazaki, M. Kogo, K. Ozono, Signaling of extracellular inorganic phosphate up-regulates cyclin D1 expression in proliferating chondrocytes via the Na+/Pi cotransporter Pit-1 and Raf/MEK/ERK pathway, Bone 47 (5) (2010) 938–947.
[31] G.R. Beck Jr., B. Zerler, E. Moran, Phosphate is a specific signal for induction of osteopontin gene expression, Proc. Natl. Acad. Sci. U. S. A. 97 (15) (2000) 8352–8357.
[32] M.L. Noonan, K.E. White, FGF23 synthesis and activity, Curr. Mol. Biol. Rep. 5 (1) (2019) 18–25.
[33] T. Michigami, Roles of osteocytes in phosphate metabolism, Front. Endocrinol. (Lausanne) 13 (2022) 967774.
[34] T.O. Carpenter, M.P. Whyte, E.A. Imel, A.M. Boot, W. Hogler, A. Linglart, R. Padidela, W. Van't Hoff, M. Mao, C.Y. Chen, A. Skrinar, E. Kakkis, J. San Martin, A.A. Portale, Burosumab therapy in children with X-linked hypophosphatemia, N. Engl. J. Med. 378 (21) (2018) 1987–1998.
[35] E.A. Imel, F.H. Glorieux, M.P. Whyte, C.F. Munns, L.M. Ward, O. Nilsson, J. H. Simmons, R. Padidela, N. Namba, H.I. Cheong, P. Pitukcheewanont, E. Sochett, W. Hogler, K. Muroya, H. Tanaka, G.S. Gottesman, A. Biggin, F. Perwad, M. Mao, C. Y. Chen, A. Skrinar, J. San Martin, A.A. Portale, Burosumab versus conventional therapy in children with X-linked hypophosphataemia: a randomised, active-controlled, open-label, phase 3 trial, Lancet 393 (10189) (2019) 2416–2427.
[36] K. Briot, A.A. Portale, M.L. Brandi, T.O. Carpenter, H.I. Cheong, M. Cohen-Solal, R. K. Crowley, R. Eastell, Y. Imanishi, S. Ing, K. Insogna, N. Ito, S. Jan de Beur, M. K. Javaid, P. Kamenicky, R. Keen, T. Kubota, R.H. Lachmann, F. Perwad, P. Pitukcheewanont, S.H. Ralston, Y. Takeuchi, H. Tanaka, T.J. Weber, H.W. Yoo, A. Nixon, M. Nixon, W. Sun, A. Williams, E.A. Imel, Burosumab treatment in adults with X-linked hypophosphataemia: 96-week patient-reported outcomes and ambulatory function from a randomised phase 3 trial and open-label extension, RMD Open 7 (3) (2021).
[37] S. Fukumoto, FGF23-related hypophosphatemic rickets/osteomalacia: diagnosis and new treatment, J. Mol. Endocrinol. 66 (2) (2021) R57–R65.
[38] E.A. Imel, Enthesopathy, osteoarthritis, and mobility in X-linked Hypophosphatemia1, J. Clin. Endocrinol. Metab. 105 (7) (2020).
[39] I. Endo, S. Fukumoto, K. Ozono, N. Namba, H. Tanaka, D. Inoue, M. Minagawa, T. Sugimoto, M. Yamauchi, T. Michigami, T. Matsumoto, Clinical usefulness of measurement of fibroblast growth factor 23 (FGF23) in hypophosphatemic patients: proposal of diagnostic criteria using FGF23 measurement, Bone 42 (6) (2008) 1235–1239.
[40] S.S. Beck-Nielsen, K. Brixen, J. Gram, C. Molgaard, High bone mineral apparent density in children with X-linked hypophosphatemia, Osteoporos. Int. 24 (8) (2013) 2215–2221.
[41] G. de Paula Colares Neto, R.M.R. Pereira, J.C. Alvarenga, L. Takayama, M.F. de Assis Funari, R.M. Martin, Evaluation of the trabecular bone score in 35 children and adults with X-linked hypophosphatemic rickets, J. Bone Miner. Metab. 41 (5) (2023) 666–672.
[42] J.L. Millan, The role of phosphatases in the initiation of skeletal mineralization, Calcif. Tissue Int. 93 (4) (2013) 299–306.
[43] S.K. Murali, O. Andrukhova, E.L. Clinkenbeard, K.E. White, R.G. Erben, Excessive Osteocytic Fgf23 secretion contributes to pyrophosphate accumulation and mineralization defect in Hyp mice, PLoS Biol. 14 (4) (2016) e1002427.
[44] S.K. Murali, P. Roschger, U. Zeitz, K. Klaushofer, O. Andrukhova, R.G. Erben, FGF23 regulates bone mineralization in a 1,25(OH)2 D3 and Klotho-independent manner, J. Bone Miner. Res. 31 (1) (2016) 129–142.
[45] A. Buck, V.M. Prade, T. Kunzke, R.G. Erben, A. Walch, Spatial metabolomics reveals upregulation of several pyrophosphate-producing pathways in cortical bone of Hyp mice, JCI Insight 7 (20) (2022).
[46] P.S. Rowe, I.R. Garrett, P.M. Schwarz, D.L. Carnes, E.M. Lafer, G.R. Mundy, G. E. Gutierrez, Surface plasmon resonance (SPR) confirms that MEPE binds to PHEX via the MEPE-ASARM motif: a model for impaired mineralization in X-linked rickets (HYP), Bone 36 (1) (2005) 33–46.
[47] N. Reznikov, B. Hoac, D.J. Buss, W.N. Addison, N.M.T. Barros, M.D. McKee, Biological stenciling of mineralization in the skeleton: local enzymatic removal of inhibitors in the extracellular matrix, Bone 138 (2020) 115447.
[48] G.R. Beck Jr., N. Knecht, Osteopontin regulation by inorganic phosphate is ERK1/2-, protein kinase C-, and proteasome-dependent, J. Biol. Chem. 278 (43) (2003) 41921–41929.
[49] T. Komori, Whole aspect of Runx2 functions in skeletal development, Int. J. Mol. Sci. 23 (10) (2022).
[50] T. Miyazaki, N. Kanatani, S. Rokutanda, C. Yoshida, S. Toyosawa, R. Nakamura, S. Takada, T. Komori, Inhibition of the terminal differentiation of odontoblasts and their transdifferentiation into osteoblasts in Runx2 transgenic mice, Arch. Histol. Cytol. 71 (2) (2008) 131–146.
[51] B.A. Byers, G.K. Pavlath, T.J. Murphy, G. Karsenty, A.J. Garcia, Cell-type-dependent up-regulation of in vitro mineralization after overexpression of the osteoblast-specific transcription factor Runx2/Cbfal, J. Bone Miner. Res. 17 (11) (2002) 1931–1944.
[52] C.A. Gersbach, B.A. Byers, G.K. Pavlath, A.J. Garcia, Runx2/Cbfa1 stimulates transdifferentiation of primary skeletal myoblasts into a mineralizing osteoblastic phenotype, Exp. Cell Res. 300 (2) (2004) 406–417.
[53] Y. Takashi, H. Kosako, S. Sawatsubashi, Y. Kinoshita, N. Ito, M.K. Tsoumpra, M. Nangaku, M. Abe, M. Matsuhisa, S. Kato, T. Matsumoto, S. Fukumoto, Activation of unliganded FGF receptor by extracellular phosphate potentiates proteolytic protection of FGF23 by its O-glycosylation, Proc. Natl. Acad. Sci. U. S. A. 116 (23) (2019) 11418–11427.
[54] S.P. Persengiev, M.R. Green, The role of ATF/CREB family members in cell growth, survival and apoptosis, Apoptosis 8 (3) (2003) 225–228.
[55] R. Zhang, J.R. Edwards, S.Y. Ko, S. Dong, H. Liu, B.O. Oyajobi, C. Papasian, H. W. Deng, M. Zhao, Transcriptional regulation of BMP2 expression by the PTH-CREB signaling pathway in osteoblasts, PLoS One 6 (6) (2011) e20780.
[56] K.H. Park, Y. Choi, D.S. Yoon, K.M. Lee, D. Kim, J.W. Lee, Zinc promotes osteoblast differentiation in human mesenchymal stem cells via activation of the cAMP-PKA-CREB signaling pathway, Stem Cells Dev. 27 (16) (2018) 1125–1135.
[57] W. Yu, F.C. Chen, W.N. Xu, S.L. Ding, P.B. Chen, L. Yang, S.D. Jiang, X.Y. Pan, Inhibition of Y1 receptor promotes osteogenesis in bone marrow stromal cells via cAMP/PKA/CREB pathway, Front. Endocrinol. (Lausanne) 11 (2020) 583105.
[58] D. Miao, B. He, Y. Jiang, T. Kobayashi, M.A. Soroceanu, J. Zhao, H. Su, X. Tong, N. Amizuka, A. Gupta, H.K. Genant, H.M. Kronenberg, D. Goltzman, A.C. Karaplis, Osteoblast-derived PTHrP is a potent endogenous bone anabolic agent that modifies the therapeutic efficacy of administered PTH 1-34, J. Clin. Invest. 115 (9) (2005) 2402–2411.
[59] N. Ansari, P.W. Ho, B. Crimeen-Irwin, I.J. Poulton, A.R. Brunt, M.R. Forwood, P. Divieti Pajevic, J.H. Gooi, T.J. Martin, N.A. Sims, Autocrine and paracrine regulation of the murine skeleton by osteocyte-derived parathyroid hormone-related protein, J. Bone Miner. Res. 33 (1) (2018) 137–153.
[60] K. Jahn, S. Kelkar, H. Zhao, Y. Xie, L.M. Tiede-Lewis, V. Dusevich, S.L. Dallas, L. F. Bonewald, Osteocytes acidify their microenvironment in response to PTHrP in vitro and in lactating mice in vivo, J. Bone Miner. Res. 32 (8) (2017) 1761–1772.
[61] P.J. Marie, F.H. Glorieux, Relation between hypomineralized periosteocytic lesions and bone mineralization in vitamin D-resistant rickets, Calcif. Tissue Int. 35 (4–5) (1983) 443–448.
[62] G. Boileau, H.S. Tenenhouse, L. Desgroseillers, P. Crine, Characterization of PHEX endopeptidase catalytic activity: identification of parathyroid-hormone-related peptide107-139 as a substrate and osteocalcin, PPi and phosphate as inhibitors, Biochem. J. 355 (Pt 3) (2001) 707–713.
[63] J.S. Adams, M.A. Gacad, F.R. Singer, Specific internalization and action of 1,25-dihydroxyvitamin D3 in cultured dermal fibroblasts from patients with X-linked hypophosphatemia, J. Clin. Endocrinol. Metab. 59 (3) (1984) 556–560.
[64] B.R. Coyac, B. Hoac, P. Chafey, G. Falgayrac, L. Slimani, P.S. Rowe, G. Penel, A. Linglart, M.D. McKee, C. Chaussain, C. Bardet, Defective mineralization in X-linked hypophosphatemia dental pulp cell cultures, J. Dent. Res. 97 (2) (2018) 184–191.

Supplemental Table and Figures

SUPPLEMENTAL TABLE

Supplemental Table S1. Primer sequences utilized in genomic PCR and RT-PCR.

SUPPLEMENTAL FIGURES

Supplemental Figure S1. Similar viability/cytotoxicity between *PHEX*-KO #2 and isogenic control iPSCs.

Supplemental Figure S2. Enhanced mineralization, increased extracellular PPi and reduced TNSALP activity in osteoblast lineage cells derived from *PHEX*-KO #2 iPSCs.

Supplemental Figure S3. Comparison of gene expression between osteoblast lineage cells differentiated from *PHEX*-KO #2 iPSCs and those from isogenic control iPSCs.

Supplemental Figure S4. Enhanced phosphorylation of CREB and increased expression of *PTHRP* in osteoblast lineage cells differentiated from *PHEX*-KO #2 iPSCs.

Supplemental Figure S5. Comparison of gene responses to extracellular Pi between osteoblast lineage cells derived from *PHEX*-KO #2 iPSCs and those from isogenic control iPSCs.

SUPPLEMENTAL TABLE

Supplemental Table S1. Primer sequences utilized in genomic PCR and RT-PCR.

Primer name	Sequence **(5′−3′)**
Ex1a-F	CTTGAAGTGGGTCCGGTGAA
Ex1b-F	GTAGAAGAGCAAGAAAGCCTT
Int1-R	ACACCACCTATGAACGCAGG
Ex2-F	GAGTCAAGGTCTCTTAAGTC
Ex3-R	TATCACAAGGATCCACAGAC
Int3-R	TAAAGTGTATCACCAAACCCC
Ex5-R	AATTGCTGTATTGACCACGAAA

SUPPLEMENTAL FIGURES

Supplemental Figure S1

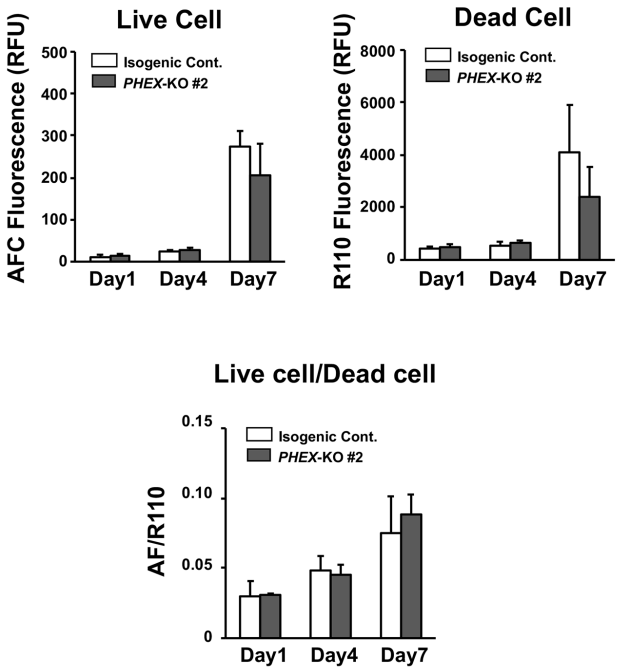

Supplemental Figure S1. Similar viability/cytotoxicity between *PHEX*-KO #2 and isogenic control iPSCs. *PHEX*-KO #2 and isogenic control iPSCs were plated at 0.5×10^3 cells/well on 96-well plates and cultured for up to 7 days. The numbers of live cells and dead cells were assessed at the indicated time points using a MultiTox-Fluor Multiplex Cytotoxicity Assay. The AFC/R110 ratio was calculated as an index for the ratio of live cells to dead cells. Data are shown as the mean ± SD (n=4). No significant differences were observed in any parameters between *PHEX*-KO #2 and isogenic control iPSCs.

Supplemental Figure S2

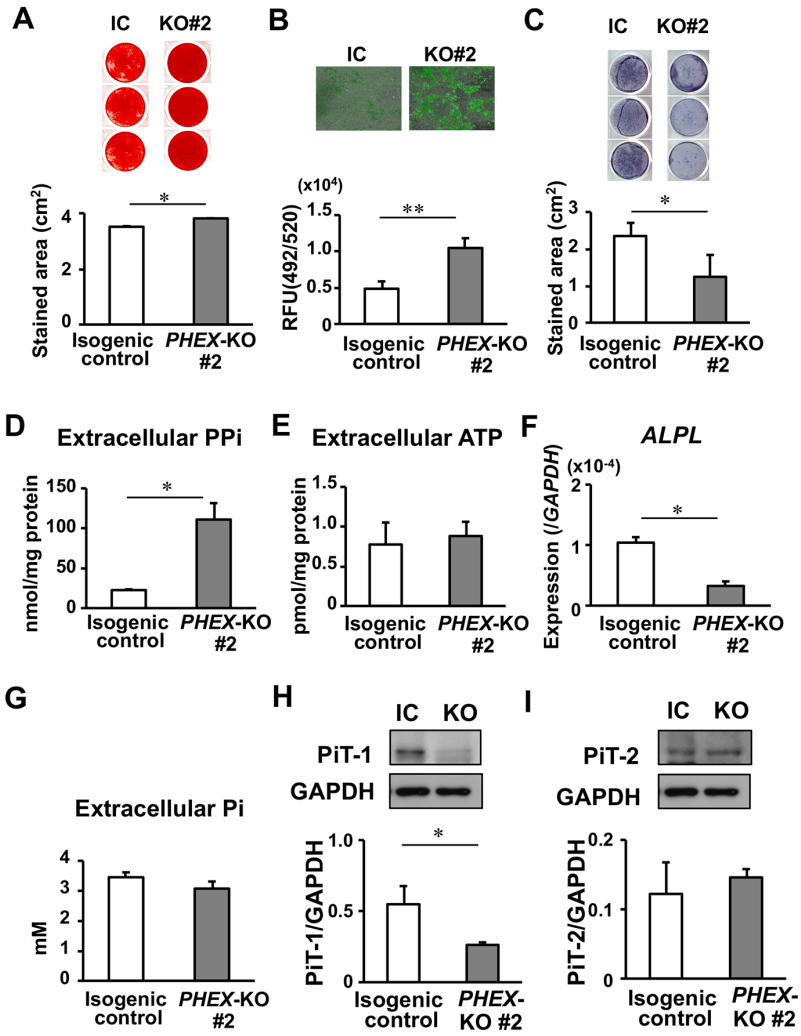

Supplemental Figure S2. Enhanced mineralization, increased extracellular PPi and reduced TNSALP activity in osteoblast lineage cells derived from *PHEX*-KO #2 iPSCs. *PHEX*-KO #2 and isogenic control iPSCs were induced to differentiate into the osteoblast lineage for 49 days. **(A)** Alizarin red staining and quantification of the stained area. **(B)** Staining and quantification of hydroxyapatite by the OsteoImage™ assay. **(C)** Staining for TNSALP activity and quantification of the stained area. **(D, E)** The extracellular levels of PPi (D) and ATP (E) in 72-hour conditioned media (CM). **(F)** The expression of *ALPL* assessed by real-time PCR. **(G)** The extracellular levels of Pi in 72-hour CM. **(H, I)** Western blotting for the expression of type III Na^+/Pi co-transporters PiT-1 (H) and PiT-2 (I). The results of densitometry are shown in the bottom graphs. Data in the graphs are shown as the mean ± SD (n=3). *, $p<0.05$ and **, $p<0.01$.

Supplemental Figure S3

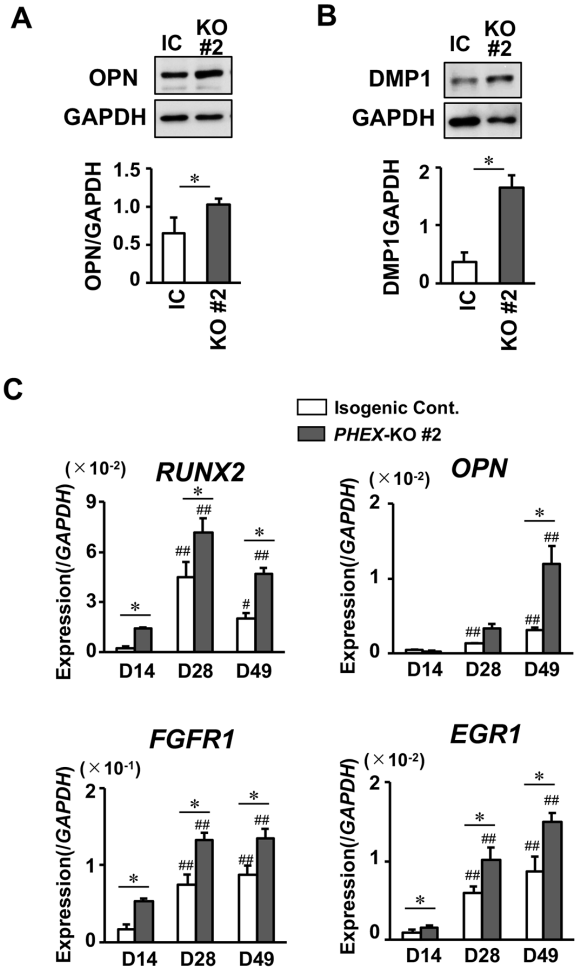

Supplemental Figure S3. Comparison of gene expression between osteoblast lineage cells differentiated from *PHEX*-KO #2 iPSCs and those from isogenic control iPSCs. *PHEX*-KO #2 and isogenic control iPSCs were induced to differentiate into the osteoblast lineage cells. **(A, B)** Western blotting for the protein expression of OPN on Day 28 (A) and DMP1 on Day 49 (B). The results of densitometry are shown in the bottom graphs. **(C)** Real-time PCR for the expression of *RUNX2*, *OPN*, *FGFR1*, and *EGR1* on the indicated time points. The copy number of target cDNA was normalized based on that of *GAPDH*. Data in the graphs are shown as the mean ± SD (n=3). $^{\#}$, $P<0.05$; $^{\#\#}$, $P<0.01$ vs Day 14. ∗, $p<0.05$.

Supplemental Figure S4

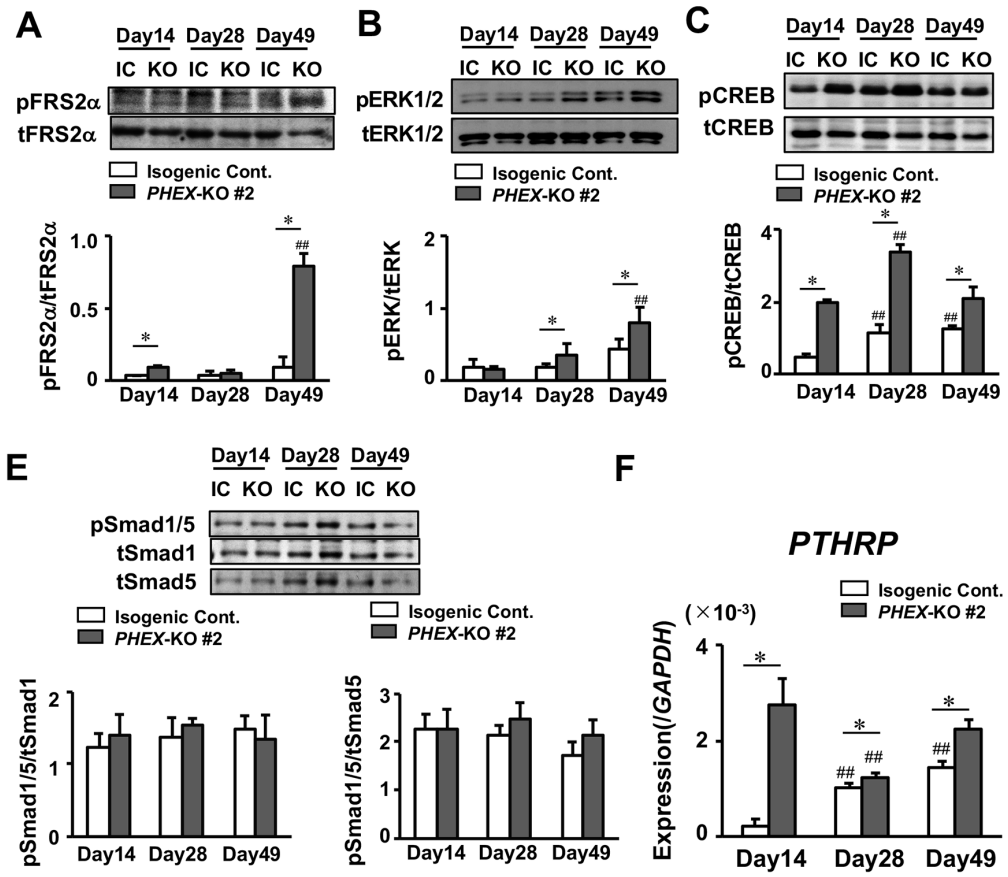

Supplemental Figure S4. Enhanced phosphorylation of CREB and increased expression of *PTHRP* in osteoblast lineage cells differentiated from *PHEX*-KO #2 iPSCs. *PHEX*-KO #2 and isogenic control iPSCs were induced to differentiate into the osteoblast lineage, and cells were harvested at the indicated time points. **(A-D)** Western blotting was performed to examine the phosphorylation of FRS2α at Tyr196 (A), ERK1/2 at Tyr180/Tyr182 (B), CREB at Ser133 (C), and Smad1 and Smad5 at Ser463 and Ser465 (D) The results of densitometry are shown in the bottom panels. **(E)** Real-time PCR for the expression of *PTHRP*. Data in the graphs are shown as the mean ± SD (n=3). $^{\#}$, $P<0.05$; $^{\#\#}$, $P<0.01$ vs Day 14. ∗, $p<0.05$.

Supplemental Figure S5

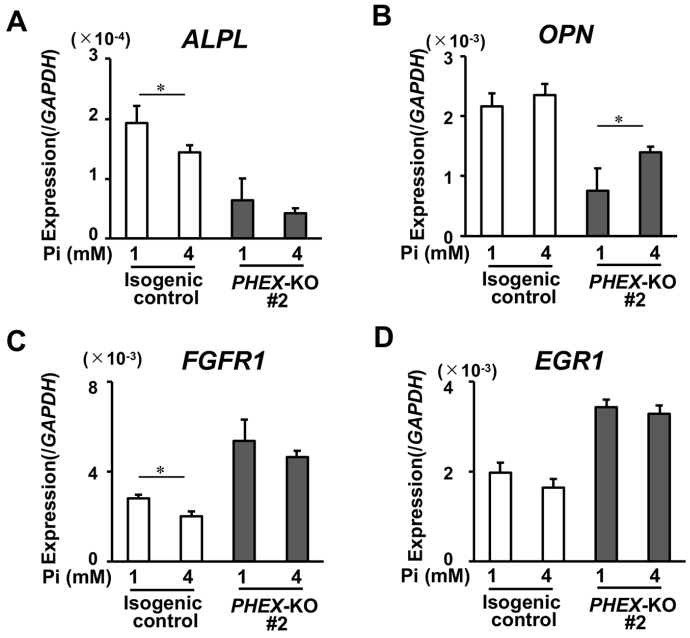

Supplemental Figure S5. Comparison of gene responses to extracellular Pi between osteoblast lineage cells derived from *PHEX*-KO #2 iPSCs and those from isogenic control iPSCs. *PHEX*-KO #2 and isogenic control iPSCs were induced to differentiate into the osteoblast lineage. On Day 42, the OI medium was changed to media containing 1 mM Pi or 4 mM Pi instead of β-glycerophosphate, and cells were cultured for an additional 7 days. On Day 49, cells were harvested for real-time PCR to analyze the expression of *ALPL* **(A)**, *OPN* **(B)**, *FGFR1* **(C)**, and *EGR1* **(D)**. Data are shown as the mean ± SD (n=3). *, $p<0.05$.

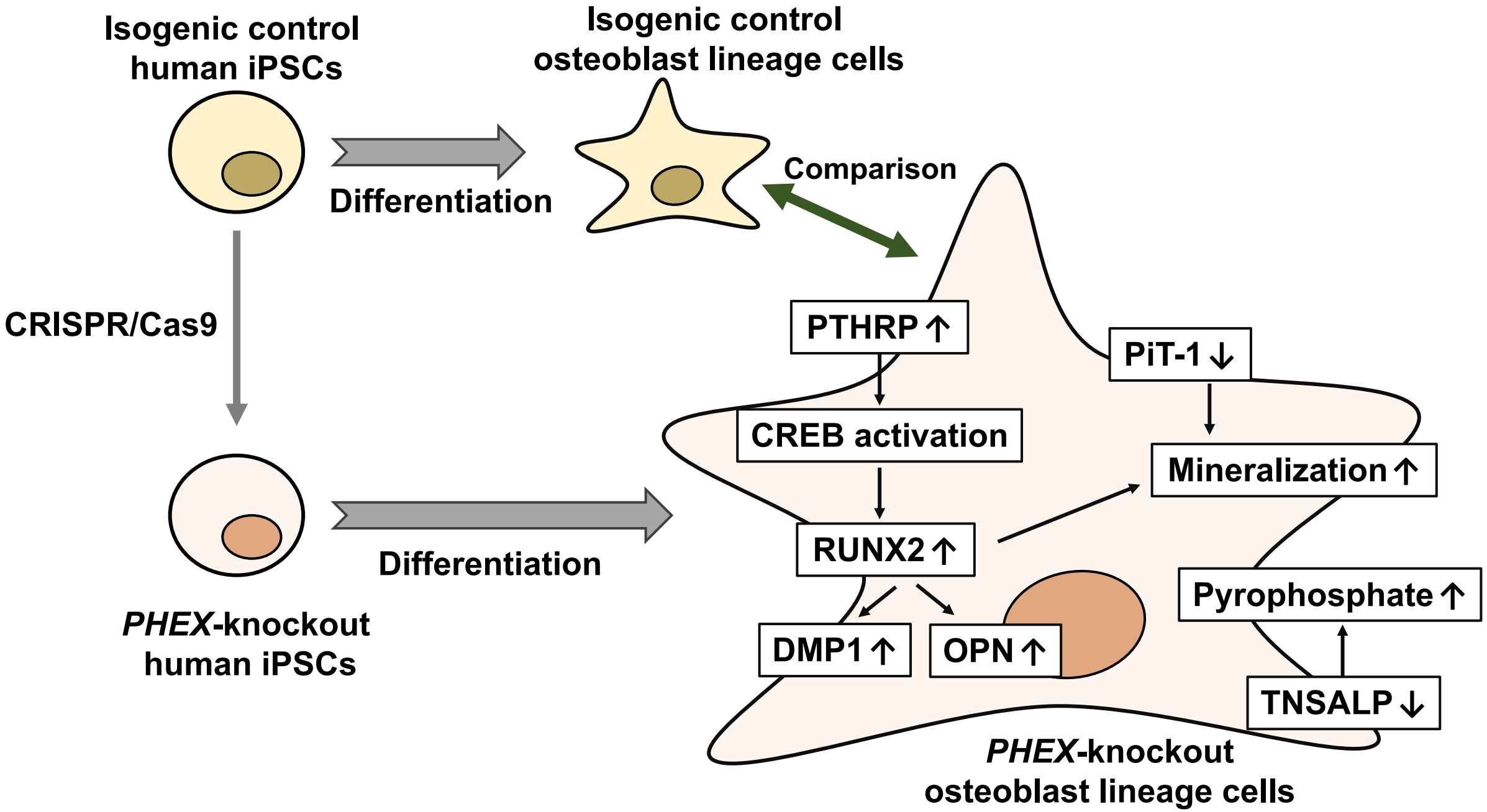
Isogenic control human iPSCs
Isogenic control osteoblast lineage cells
Differentiation
Comparison
CRISPR/Cas9
PTHRP ↑
PiT-1 ↓
CREB activation
Mineralization ↑
RUNX2 ↑
Differentiation
Pyrophosphate ↑
DMP1 ↑
OPN ↑
TNSALP ↓
PHEX-knockout human iPSCs
PHEX-knockout osteoblast lineage cells